
This is the **published version** of the master thesis:

Cortés Ros, Brian; García García, Joan J. , dir. Comparison of common ultra-low power harvesting RF rectifier circuits. 2022. 76 pag. (1170 Màster Universitari en Enginyeria de Telecomunicació / Telecommunication Engineering)

This version is available at <https://ddd.uab.cat/record/259440>

under the terms of the  license



A Thesis for the

Master in Telecommunication Engineering

Comparison of common ultra-low power
harvesting RF rectifier circuits

by
Brian Cortés Ros

Supervisor: Joan J. García García

Electronic Engineering Department

**Escola d'Enginyeria
Universitat Autònoma de Barcelona (UAB)**

January 2022



El sotasignant, *Joan J. García García*, Professor del Departament d'Enginyeria Electrònica de l'Escola d'Enginyeria de la Universitat Autònoma de Barcelona (UAB),

CERTIFICA:

Que el projecte presentat en aquesta memòria de Treball Final de Master ha estat realitzat sota la seva direcció per l'alumne *Brian Cortés Ros*.

I, perquè consti a tots els efectes, signa el present certificat.

Bellaterra, *17 Enero 2022*

Signatura:

Resum: *En aquest projecte s'analitza i compara diferents tipus de circuits rectificadors comuns de RF Harvesting per ultra baixa potencia. S'ha utilitzat una antena com element de captació d'energia i s'ha analitzat la potencia disponible en el ambient, concretament en els laboratoris GAEMI de la UAB. Las simulacions s'han realitzat amb el software Keysight ADS. S'ha demostrat, mitjançant la simulació, que el rectificador simple mostra una major eficiència respecte als demás rectificadores i que el valor de la resistència de carga es el element predominant en el càlcul de la eficiència. S'ha confirmat experimentalment que les mesures no es desvien tant de les mesures simulades. Els resultats obtinguts son susceptibles de ser aplicats en la generació de prototips de sistemes Harvesting de RF.*

Resumen: *En este proyecto se ha analizado y comparado diferentes tipos de circuitos rectificadores comunes de RF Harvesting para ultra baja potencia. Se ha utilizado una antena como elemento de captación de la energía y se ha analizado la potencia disponible en el ambiente, concretamente en los laboratorios GAEMI de la UAB. Las simulaciones se han realizado mediante el software Keysight ADS. Se ha demostrado, mediante la simulación, que el rectificador simple muestra una eficiencia mayor respecto a los demás rectificadores y que el valor de la resistencia de carga es el elemento predominante en el cálculo de esta eficiencia. Se ha confirmado experimentalmente que las medidas no se desvían de las medidas simuladas. Los resultados obtenidos son susceptibles de ser aplicados en la generación de prototipos de sistemas Harvesting de RF.*

Summary: *This project has analysed and compared different types of common RF Harvesting rectifier circuits for ultra-low power. An antenna has been used as an energy harvesting element and the power available in the environment has been analysed, specifically in the GAEMI laboratories of the UAB. The simulations were carried out using the Keysight ADS software. It has been demonstrated, by means of simulation, that the simple rectifier shows a higher efficiency than the other rectifiers and that the value of the load resistance is the predominant element in the calculation of this efficiency. It has been experimentally confirmed that the measurements do not deviate from the simulated measurements. The results obtained can be applied to the generation of prototypes of RF Harvesting systems.*

Index

1.INTRODUCTION	1
1.1 MOTIVATION	1
1.2 OBJECTIVES	2
1.3 STATE OF THE ART	2
2. THEORETICAL CONCEPTS.....	5
2.1 MAXWELL EQUATIONS	5
2.2 ELECTROMAGNETIC WAVES.....	6
2.3 RF ENERGY HARVESTING.....	7
2.4 DIODE.....	9
2.5 RECTIFIER CIRCUITS	12
2.5.1 Simple Rectifier	13
2.5.2 Bridge.....	14
2.5.3 Dickson- Greinach N=1	15
2.5.4 Dickson N	17
2.5.5 Greinach N=2.....	18
2.5.6 Full wave Dickson Variation	19
3. SIMULATED AND EXPERIMENTAL RESULTS	21
3.1 SET UP.....	21
3.1.1 Spectrum analyser.....	21
3.1.2 Antenna Model.....	24
3.2 VIRTUAL SET UP	25
3.2.1 ADS.....	25
3.2.2 Estructure components ADS.....	26
3.3 AMBIENT AVAILABLE POWER FOR RF HARVESTING.....	29
3.4 RECTIFIER CIRCUITS SIMULATED RESULTS.....	32
4. ANALYSIS AND DISCUSSION.....	47
5. CONCLUSION	55
6. REFERENCES	57
7. ANNEX.....	63
ANNEX I. DATASHEET ANTENNA ANT-24G-HL90-SMA	63
ANNEX II. DATASHEET DIODE SCHOTTKY SMS7630_079	64

List of Figures

Figure 1: Conceptual block diagram of an RF power Harvesting System [6].	3
Figure 2: RF input power for Schottky diode operation [7].	4
Figure 3: Propagation of an electromagnetic wave.	6
Figure 4 : Impedance Matching.	8
Figure 5: I-V curve of a diode.	9
Figure 6: Operational regions.	9
Figure 7: Evolution of rectification based on the technology used by diodes.	10
Figure 8: Junction Diode Schottky	11
Figure 9: Comparison of I-V Characteristics.	12
Figure 10: Half Wave Rectifier Circuit.	13
Figure 11: Full Wave Rectifier Circuit.	13
Figure 12: Simple Rectifier with Capacitor [14].	14
Figure 13: Bridge Rectifier [17].	14
Figure 14: Half Wave Voltage Doubler (Dickson-Greinach N=1) [18].	15
Figure 15: Waveform of voltage doubler [19].	16
Figure 16: Original Dickson Charge Pump [20].	17
Figure 17: 2-Stage Dickson Charge Pump [21].	18
Figure 18: DC Voltage Quadrupler Circuit (Greinach N=2) [22].	18
Figure 19: Configuration of the novel full-wave Greinacher rectifying circuit [23].	19
Figure 20: Spectrum analyser Rohde Schwarz R&S®FSL [24].	21
Figure 21: Block diagram of the spectrum analyser[25].	22
Figure 22: Spectrum analyser representation of the units on abscissa axis (frequency (Hz)) and coordinate axis (dBm)[26].	22
Figure 23: ANT-24-GHL90-SMA.	24
Figure 24: Configuration Harmonic Balance Parameters in Keysight ADS.	25
Figure 25: Configuration Parameter Sweep in Keysight ADS.	26
Figure 26: ADS diode specifications.	27
Figure 27: Schottky Design Model for the HB Analysis..	27
Figure 28: Symbol diode SMS7630_079.	27
Figure 29: One Tone Power Source ADS.	28
Figure 30: Load Resistance Symbol.	28

Figure 31: Capacity symbol.	29
Figure 32: ANT-24G-HL90-SMA power capture over 24h with respect to frequency.	31
Figure 33: Simple Diode Capacitor Rectifier ADS.	33
Figure 34: a) Representation (simple rectifier) of the efficiency with respect to the input power for each value of the load resistance. b) Topographical efficiency map for the simple rectifier.	34
Figure 35: a) Representation (simple rectifier) of the output voltage with respect to the input power for each value of the load resistance. b) Topographical voltage map for the simple rectifier.	34
Figure 36: Representation of simple rectifier input impedance (magnitude (top) and phase (bottom)), with respect to the input power.	35
Figure 37: Bridge Rectifier ADS.	35
Figure 38: a) Representation (Bridge rectifier) of the efficiency with respect to the input power for each value of the load resistance. b) Topographical efficiency map for the Bridge rectifier.	36
Figure 39: a) Representation (Bridge rectifier) of the output voltage with respect to the input power for each value of the load resistance. b) Topographical voltage map for the Bridge rectifier.	36
Figure 40: Representation of Bridge rectifier input impedance (magnitude (top) and phase (bottom)), with respect to the input power.	37
Figure 41: Dickson- Greinach $N=1$ Rectifier.	37
Figure 42: a) Representation (Dickson- Greinach rectifier) of the efficiency with respect to the input power for each value of the load resistance. b) Topographical efficiency map for the Dickson- Greinach.	38
Figure 43: a) Representation (Dickson- Greinach rectifier) of the output voltage with respect to the input power for each value of the load resistance. b) Topographical voltage map for the Dickson- Greinach rectifier.	38
Figure 44: Representation of Dickson- Greinach rectifier input impedance (magnitude (top) and phase (bottom)), with respect to the input power.	39
Figure 45: Dickson N rectifier ADS.	39
Figure 46: a) Representation (Dickson N rectifier) of the efficiency with respect to the input power for each value of the load resistance. b) Topographical efficiency map for the Dickson N	40

Figure 47: a) Representation (Dickson N rectifier) of the output voltage with respect to the input power for each value of the load resistance. b) Topographical voltage map for the Dickson N rectifier.	40
Figure 48: Representation of Dickson N rectifier input impedance (magnitude (top) and phase (bottom)), with respect to the input power.	41
Figure 49: Greinach N=2 Rectifier.	41
Figure 50: a) Representation (Greinach N=2rectifier) of the efficiency with respect to the input power for each value of the load resistance. b) Topographical efficiency map for the Greinach N=2.	42
Figure 51: a) Representation (Greinach N=2 rectifier) of the output voltage with respect to the input power for each value of the load resistance. b) Topographical voltage map for the Greinach N=2rectifier.	42
Figure 52: Representation of Greinach N=2rectifier input impedance (magnitude (top) and phase (bottom)), with respect to the input power.	43
Figure 53: Full wave Dickson Variation rectifier.	43
Figure 54: a) Representation (Full wave Dickson Variation rectifier) of the efficiency with respect to the input power for each value of the load resistance. b) Topographical efficiency map for the Full wave Dickson Variation.	44
Figure 55: a) Representation (Full wave Dickson Variation rectifier) of the output voltage with respect to the input power for each value of the load resistance. b) Topographical voltage map for the Full wave Dickson Variation rectifier.	44
Figure 56: Representation of Greinach N=2rectifier input impedance (magnitude (top) and phase (bottom)), with respect to the input power.	45
Figure 57: (a) Simulated rectifier efficiency for the six circuits of P_{nom} for a $RL = 10\text{ k}\Omega$ (b) Simulated rectifier efficiency for the six circuits of P_{in} for a $RL = 10\text{ k}\Omega$	50
Figure 58: (a) Simulated rectifier efficiency for the six circuits of P_{in} for a $RL = 100\Omega$. (b) Simulated rectifier efficiency for the six circuits of P_{in} for a $RL = 100\text{ k}\Omega$	51
Figure 59: Experimental setup and details of the rectifier prototype implementation.	52
Figure 60: Representation of the efficiency of the simulated (solid line) and experimental (dashed triangle line) rectifiers with respect to the load resistance at a fixed power of -30dBm. The three circuits are the simple rectifier, the bridge rectifier and the Dickson-Greinach rectifier.	53

List of Tables

Table 1: Maxwell Equations.	5
Table 2: ANT-24-GHL90-SMA Antenna specification.....	24
Table 3: Summary of the variables and each value in ADS.....	29
Table 4: Common RF frequency bands and its respective frequency ranges [28].....	30
Table 5: Spectrum analyser parameters for antenna characterisation.	30
Table 6: Emission power level measurements (dBm) for RF energy sources.	32
Table 7: Topographical representation of the efficiency and voltage of all implemented rectifier circuits.	48
Table 8: Comparison with the data obtained from the different rectifier circuits operating @ 2.45GHz	49

1.Introduction

1.1 Motivation

There is now a global trend towards increasing the amount energy of energy extracted from the environment and the replacement of battery power. This trend is due to the difficult disposal of the chemicals from which they are created. These are harmful to the environment as most batteries end up in landfills and cause pollution of the land and water underneath.

To continue with this worldwide objective, a balance must be found between the devices to be deployed and the energy to be captured. Due to the limitations of power generation caused by cables and the devices own losses, it is currently difficult to find an alternative technology that can replace these charging elements.

For years, studies have been carried out to find different proposals capable of offering the same performance without being so harmful. One alternative is radio-frequency Energy Harvesting, which harnesses the energy in the environment. The main problem is the low levels of energy density in the environment [1][2][3].

This field is undergoing a major evolution and, as a result, Energy Harvesting applications are expected to increase the lifetime or even achieve self-sufficient electronic systems, providing a major impetus for research growth in industries and academia.

The main motivation and focus of this project are to present detailed information on the energy captured from different very low power (mW) rectifier circuits. Since Energy Harvesting circuits are designed to operate with relatively small voltages and currents, they rely on state-of-the-art electrical technology for obtaining high efficiency.

This project will focus on the field of RF Energy Harvesting in the laboratories of the UAB's Grup d'Aplicacions Electro-Magnètiques Industrials (GAEMI).

1.2 Objectives

The main objective is to study and compare different rectifier circuits used in Energy Harvesting systems for ultra-low power use in a realistic environment using the full spectrum available.

To achieve the proposed objective, first, the available power of the environment had to be analysed by means of a spectrum analyser and a receiving antenna. Once the signal has been captured, different rectifier circuits have been designed in order to evaluate the efficiency, voltage and input impedance with respect to the input power and also taking into account the value of the load resistance. Finally, when all these data have been collected, each of the circuits will be purchased and analysed in order to find the most optimal one for this particular case.

1.3 State of the Art

The concept of wireless Energy Harvesting has been raised by Nikola Tesla and Heinrich Hertz [4]. The history of RF power Harvesting in free space originated in the late 1950s with a microwave-powered helicopter system, but later the concept of Energy Harvesting emerged as a technique of harvesting energy from the external environment using different methods such as thermoelectric conversion, vibrations, and solar energy among others.

Until then, the development of telecommunications in the last decades has been exponential, from 2G and 3G to 4G and the study of 5G where many countries are doing large-scale trials. As new base stations are deployed with this technology, more frequency bands emerge and signals become denser (a main problem is the low power density today), which will increase the available ambient radio frequency energy to be captured in space [5].

Figure 1 presents the structure of an RF Energy Harvesting system and the factors that contribute to the performance of the whole system. The three blocks that make it up are the RF source, the transmission space and Wireless power Harvesting circuit.

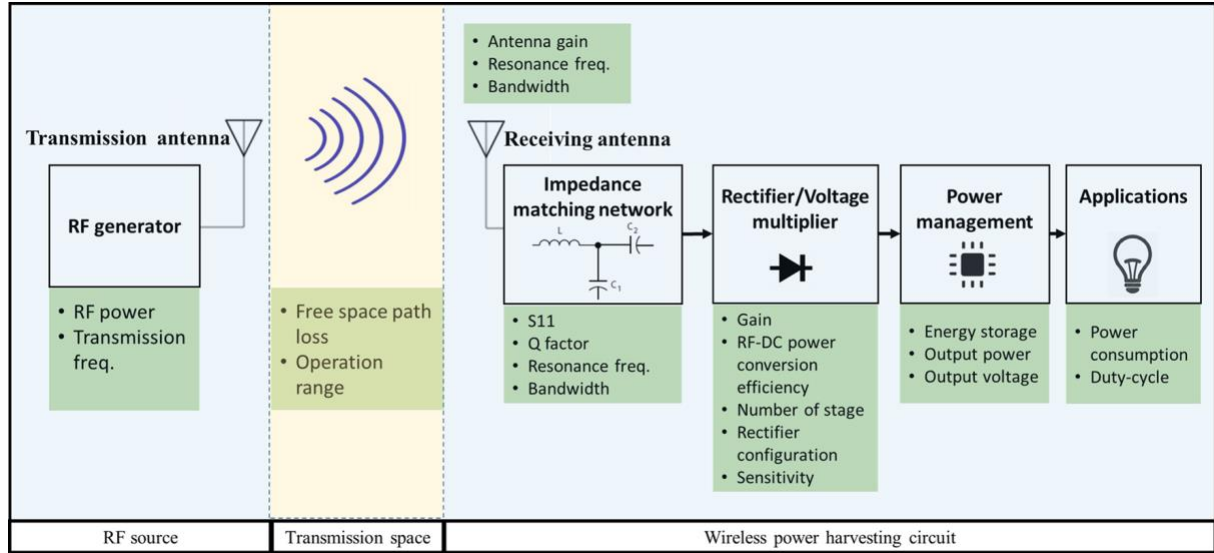


Figure 1: Conceptual block diagram of an RF power Harvesting System [6].

The first block contains the RF wave generator. This device is responsible for transmitting the RF signal through the environment. Once transmitted, this wave will travel through the second stage and will be subjected to the different losses caused by the environment. The deterioration of this wave will be caused by the distance between the transmitting antenna and the receiving antenna. In other words, the greater the distance between the two, the greater the signal loss.

The last block is the Wireless power Harvesting circuit which is characterised by its receiving antenna. The received signal passes through the impedance matching network, which is responsible for matching the impedances to achieve maximum power transfer. In the rectification stage, the RF signal is converted from RF to DC using a rectifier circuit composed of Schottky diodes. Finally, this energy is stored in capacitances.

The most critical stage of the system is the rectification process. It is for this reason that the diode, mainly the Schottky diode, becomes important. This electronic component is ideal for low-power rectifiers used in harvesting systems because of its switching speed and low threshold voltage [7].

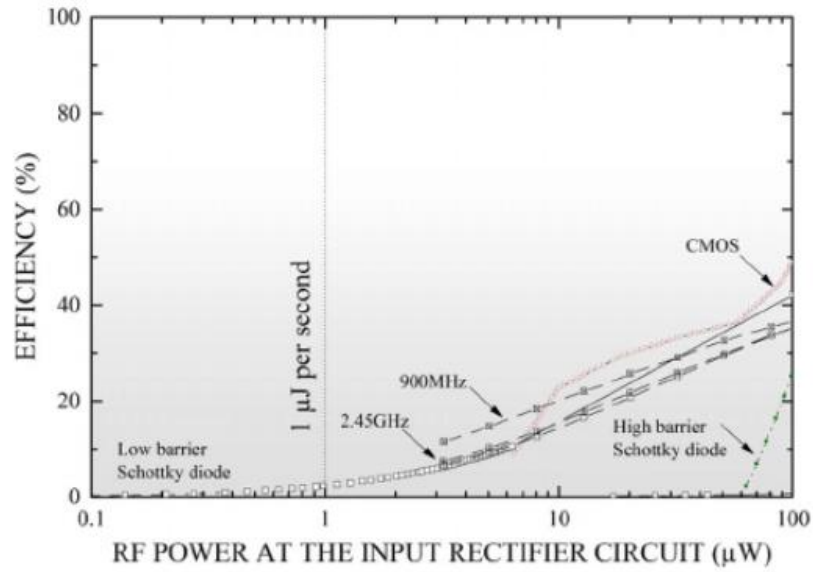


Figure 2: RF input power for Schottky diode operation [7].

Figure 2 shows the efficiency of the Schottky diode as a function of RF input power compared to CMOS transistors. Unlike CMOS transistors, Schottky diodes are able to work when the power of the receiver circuit is very low, making them very suitable for Energy Harvesting.

This project focuses on the harvesting of this type of energy. With different compositions of rectifier circuits and the use of Schottky diodes, the most efficient way of harvesting energy is sought by focusing on devices working at low power.

2. Theoretical Concepts

In this section, we will explain physical and electronic concepts that will help to understand the contents and objectives of the work. Firstly, a brief introduction to Maxwell's equations will be given. These concepts will make it easier to understand what electromagnetic waves are and how they influence radio frequency energy. A presentation of RF Energy Harvesting and the rectifier circuits that are used to capture and utilise energy from the environment is also given.

2.1 Maxwell Equations

James Clerk Maxwell took a set of experimental laws and unified them as a coherent, symmetrical set of equations known as Maxwell's equations. Maxwell's equations are a set of four differential equations that form the theoretical basis for describing classical electromagnetism:

- Gauss's law: Electric charges produce an electric field. The electric flux through a closed surface is proportional to the enclosed charge.
- Gauss's law of magnetism: There are no magnetic monopoles. The magnetic flux through a closed surface is zero.
- Faraday's Law: Time-varying magnetic fields produce an electric field.
- Ampère's Law: Stable currents and time-varying electric fields (the latter due to Maxwell's correction) produce a magnetic field.

Name	Differential form	Integral form
Gauss' law	$\vec{\nabla} \cdot \vec{E} = \frac{\rho}{\epsilon_0}$	$\oint \vec{E} \cdot d\vec{S} = \frac{\rho}{\epsilon_0}$
Gauss' law for magnetism	$\vec{\nabla} \cdot \vec{B} = 0$	$\oint \vec{B} \cdot d\vec{S} = 0$
Faraday's law of induction	$\vec{\nabla} \wedge \vec{E} = -\frac{\partial \vec{B}}{\partial t}$	$\oint \vec{E} \cdot d\vec{l} = -\frac{d}{dt} \int \vec{B} \cdot d\vec{S}$
Ampère's law	$\vec{\nabla} \wedge \vec{B} = \mu_0 \vec{J}$	$\oint \vec{B} \cdot d\vec{l} = \mu_0 \int \vec{J} \cdot d\vec{S} + \mu_0 \epsilon_0 \frac{d}{dt} \int \vec{E} \cdot d\vec{S}$

Table 1: Maxwell Equations.

Where [8]:

\vec{B} = magnetic flux density or magnetic induction (Wb/m²).

\vec{E} = electric field strength (V/m).

\vec{H} = magnetic field strength (A/m).

\vec{J} = surface current density (A/m²).

ρ = volumetric electric charge density (C/m³).

ϵ = electric permittivity (F/m)

μ = magnetic permeability (H/m).

These equations describe how electric and magnetic fields propagate, how they interact and how they are influenced by objects (Table 1).

2.2 Electromagnetic Waves

Maxwell's studies led to the understanding of electromagnetic waves through the conceptualisation of his equations. He later predicted that electromagnetic wave frequencies travel at the speed of light. He was also the first to introduce the concept of the electromagnetic spectrum.

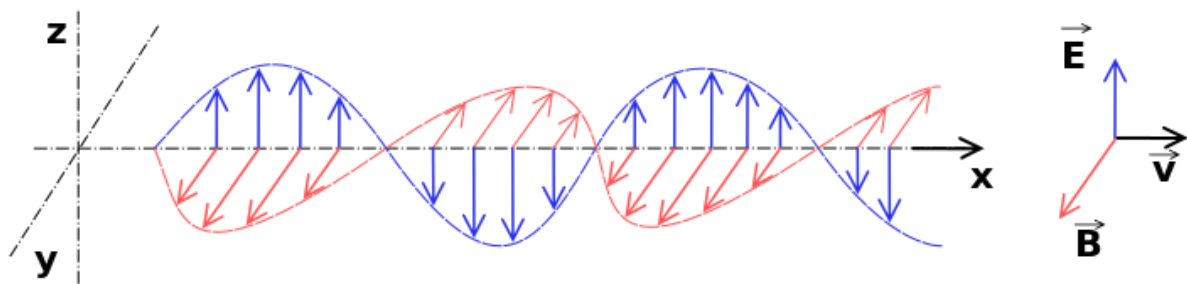


Figure 3: Propagation of an electromagnetic wave.

The type of waves created by photons are defined as electromagnetic waves that can be created by natural or artificial sources. In Figure 3, electromagnetic waves are made up of electric and magnetic force fields.

As explained below, radio frequency (RF) energy is a form of electromagnetic radiation that applies to the less energetic portion of the electromagnetic spectrum, located between 3 Hz and 300 GHz.

2.3 RF Energy Harvesting

The extraction of ambient RF energy comes from the surrounding wireless energy sources, such as mobile phone towers, broadcasting stations, RF emitting devices and Wi-Fi hotspots. There are other ways of obtaining energy from nature in alternative ways such as solar energy, wind energy, thermal energy, mechanical energy, and vibration energy.

One of the problems of RF Energy Harvesting for low power is the maximum harvesting of power from the environment to supply a system. As this power is often insufficient, one of the solutions is the use of resonant cavities [9]. This technique is commonly used in microwave engineering where electromagnetic waves are reflected from metal walls. This method allows confining the RF power in the antenna region, increasing the possibility of re-capturing the reflected energy [7].

As shown in Figure 1 above, there are different stages in RF Energy Harvesting systems. The RF energy capture stage is the most critical as the collection of RF energy presents some problems:

- The output voltage is not regulated and cannot be used directly to supply electrical circuits.
- They do not provide continuous and uninterrupted power.
- They generate very low average power.

It is for this reason that in the RF energy capture stage, microwave receiver antennas are used which are capable of collect the energy that exists in the environment.

Once the signal has been captured from the environment, a matching stage is necessary. The matching network promotes maximum power transfer. This happens when the output impedance is matched to the impedance of the connected load. The technique used to achieve this effect is impedance matching (Figure 4) [10].

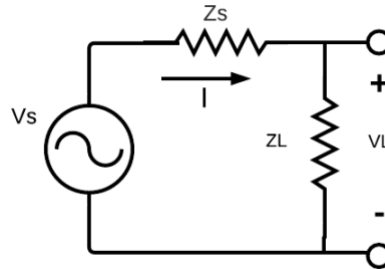


Figure 4 : Impedance Matching.

The main problem with impedance matching is that it can only be matched to one frequency, so a large amount of the spectrum picked up by the antenna is lost. The amount of energy lost can be calculated by the coefficient (1).

$$\Gamma = \frac{Z_L - Z_S}{Z_L + Z_S} \quad (1)$$

Where Z_1 Z_2 are the impedances presented by the antenna and the circuit respectively in the frequency bands of interest. The objective is to find a Γ that is equal to 0, making the input impedance equal to that of the load. This avoids a reflected wave by reducing energy loss to minimum levels.

Once the signal has passed through the impedance matching network, it is necessary to convert the radio frequency signal, alternating current signals, to direct current. Rectifier circuits are responsible for this signal conversion.

In the last stage, a battery or a capacitor is used to store the energy. The problems with the use of a battery are the long charging time, the high energy for this charge and the occupied area. Therefore, in Energy Harvesting, capacitors or supercapacitors are used as energy storage elements. These elements solve the problem of area and weight and are quick to charge.

2.4 Diode

The semiconductor diode is the most common diode used today. It is made of semiconductor crystal, such as silicon (Si), with impurities in it to create a region containing negative charge carriers (electrons), called an n-type semiconductor, and a region on the other side containing positive charge carriers, called a p-type semiconductor. Its characteristic curve (I-V) consists of two regions: below a certain potential difference it behaves as an open circuit (does not conduct), and above it as a closed circuit with a very small electrical resistance [11].

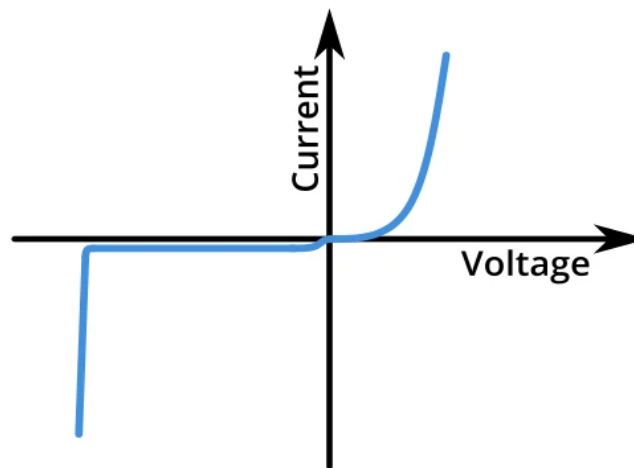


Figure 5: I-V curve of a diode.

As it can see in the Figure 5, at positive voltages, the curve rises exponentially, indicating that current is free to flow through the device. At negative voltages, the current remains nearly at zero. However, a sufficiently large negative voltage, known as the breakdown voltage, will cause the diode to become conductive to negative current. Similar to a resistor, a standard diode is a passive device, operating only within Quadrants I and III (Figure 6). It should be noted that the diode is a non-linear device because its I-V curve is not a straight line [8].

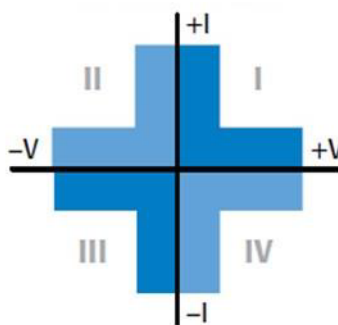


Figure 6: Operational regions.

Over the years, diodes have proven to be the most widely used technology in the rectification process due to their conversion efficiency and power management. One parameter to evaluate how good diode rectification is the Zero Bias Current Responsivity. This parameter is a direct function of the I-V characteristic curve, which relates the short-circuit current obtained by the rectification and the voltage absorbed by the PN junction resistance. The evolution of the rectifying capabilities of different types of diodes over the years can be seen in Figure 7.

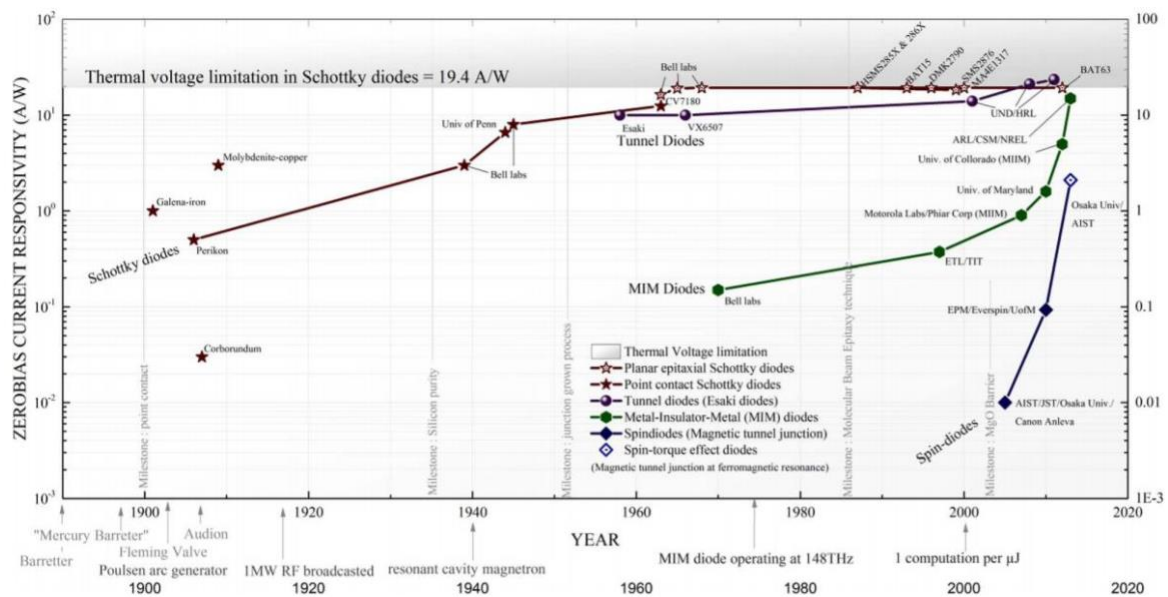


Figure 7: Evolution of rectification based on the technology used by diodes.

As can be seen in the figure above, the most widely used fabrication technology over the last century has been based on Schottky diodes.

The Schottky diode is a semiconductor diode that can be used in a wide variety of waveforming, switching and rectifying applications, just like any other junction diode. The main advantage is that the forward voltage drop of a Schottky diode is substantially lower than the 0.7V of the conventional silicon PN junction diode.

Schottky diodes have many useful applications, from rectification, signal conditioning and switching, to TTL and CMOS logic gates, mainly due to their low power consumption and fast switching speed.

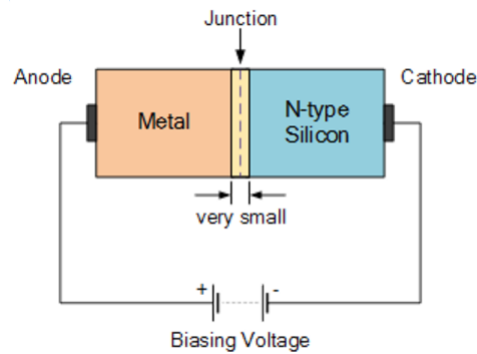


Figure 8: Junction Diode Schottky.

Figure 8 is the simplified construction of the Schottky diode in which a lightly doped n-type silicon semiconductor is bonded to a metal electrode to produce what is called a metallic semiconductor junction, known as a Schottky barrier. The width of this metal semiconductor junction will depend largely on the type of metal compound and the semiconductor material used in its construction.

When forward biased, electrons move from the n-type material to the metal electrode allowing current to pass through. Therefore, the current through the Schottky diode is the result of the drift of the majority carriers.

As there is no p-type semiconductor material and therefore no minority carriers (holes), when reverse biasing occurs, the diodes conduction stops very quickly and goes on to block current flow, as in the case of a conventional PN junction diode. Therefore, for a Schottky diode there is a very fast response to changes in bias and it demonstrates the characteristics of a rectifier diode.

This makes them much faster responding. The main characteristics of these diodes are:

- High switching speed (up to 300MHz).
- They do not have a depletion layer associated with the metal-semiconductor junction, so they do not take time to remove the charge from this layer as other diodes do when there is a change of state (on-off).
- Allows for the elimination of current peaks with fast response times.
- Low threshold voltage, approximately 0.2V to 0.4V.

Figure 9 shows the characteristic curve of the Schottky diode compared to other diodes.

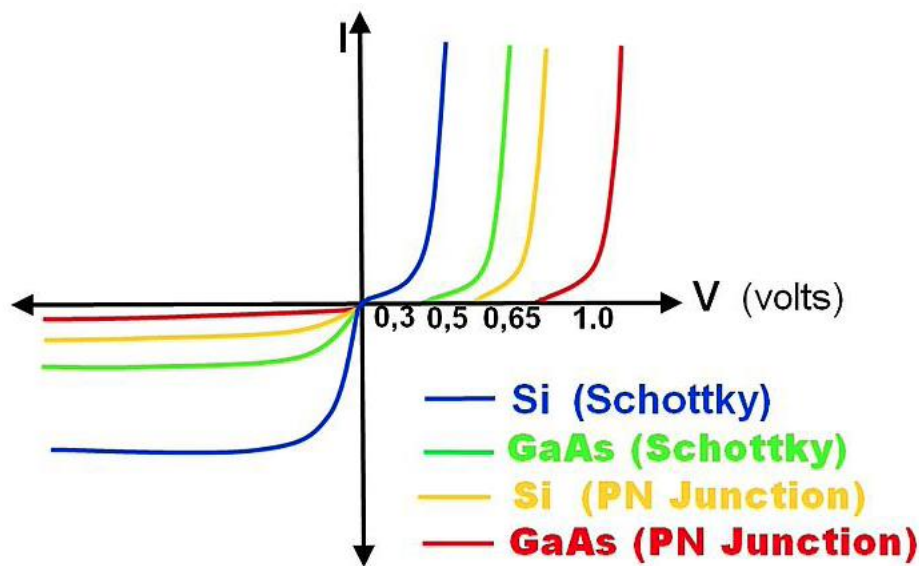


Figure 9: Comparison of I-V Characteristics.

As can be seen, the Schottky has a lower voltage drop when directly biased compared to other diodes. This characteristic is the reason why Schottky diodes are used in low-power electronic systems.

Another important difference is that the threshold voltage at which the Schottky (Si) starts to conduct is at low levels, around 0.2V-0.3V. This makes the direct current higher than other diodes. Finally, it is worth noting that the Schottky has a lower power loss, making it ideal for high current and low voltage applications.

2.5 Rectifier Circuits

A rectifier circuit converts alternating current into direct current. This is done using rectifier diodes, previously discussed.

There are two types of rectifier circuits, half-wave and full-wave rectifier circuits. A full-wave rectifier is a circuit designed to harness both half-cycles (positive and negative) of the alternating current to obtain direct current. The difference with the half-wave rectifier is that the latter only uses the positive half-cycle of the AC signal.

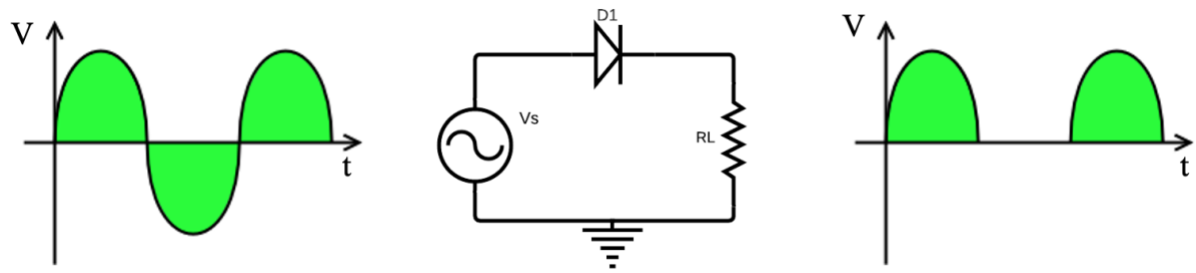


Figure 10: Half Wave Rectifier Circuit.

Figure 10 shows a half-wave rectifier where it can be seen how it takes advantage of the positive half-cycles of the signal and eliminates the negative ones.

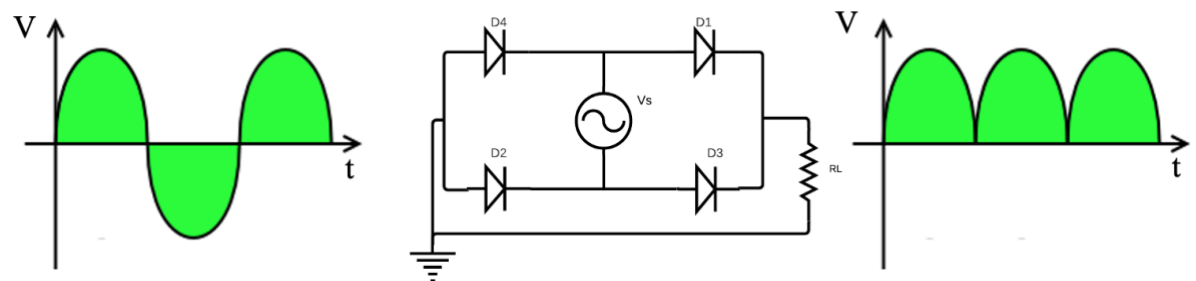


Figure 11: Full Wave Rectifier Circuit.

Figure 11 shows a full-wave rectifier where it harnesses the half-cycles by converting them both to positive. In this way it harnesses all the alternating current in the circuit and converts it to direct current.

One of the important elements of rectifier circuits, apart from the diodes, is the load resistor. The value of the resistor to be chosen depends on the type of rectifier circuit to be implemented and the maximum power to be obtained. A study of different resistor values is given below (section 3.4).

2.5.1 Simple Rectifier

The simple rectifier consists of a circuit implemented with a single diode and a load resistor. There is the possibility to add a capacitance to the circuit to obtain a better rectification. The main characteristic of single diode rectifiers is that they are more energy efficient when the available input power is very low [13].

These circuits are characterised as half-wave rectifiers. Figure 12 shows a simple rectifier with a capacitance. As can be seen, the circuit and its behaviour are very similar to Figure 12. The difference is that the capacitance means that there is no direct drop when the negative half-cycle is rectified, but a small discharge of the capacitor voltage until it reaches the next positive half-cycle of the signal again.

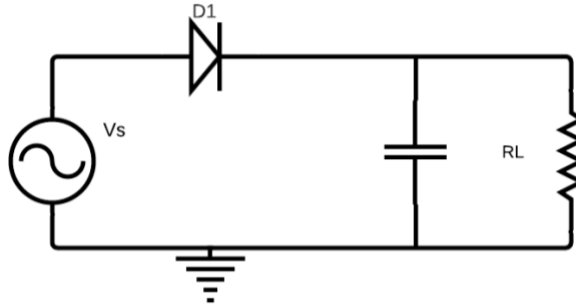


Figure 12: Simple Rectifier with Capacitor [14].

The amount of ripple voltage can be further reduced by using larger value capacitors but there are limits both on cost and size to the types of smoothing capacitors used. For a given capacitor value, a greater load current (smaller load resistance) will discharge the capacitor more quickly (RC Time Constant) and so increases the ripple obtained [15].

2.5.2 Bridge

The bridge rectifier circuit consists of four diodes, a capacitor and a load resistor. The power diodes can be connected together to form a full-wave rectifier. The alternating current flows through the diode bridge, where it is operated in half cycles. Diodes D1-D2 and D3-D4 are connected in series, but they are in reverse bias. That is, when D1-D2 are in direct D3-D4 are in reverse and vice versa [16].

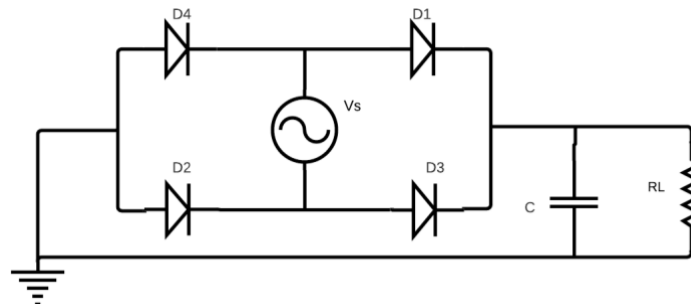


Figure 13: Bridge Rectifier [17].

Figure 13 shows the schematic of a bridge rectifier circuit. The result of the rectification is a much higher ripple than that of the simple rectifier as it takes advantage of both half-cycles.

2.5.3 Dickson- Greinach N=1

The single series diode configuration (which is different from the single shunt diode configuration) is not efficient for ambient RF Energy Harvesting since the incident power density is relatively low which does not satisfy the biasing requirement of the circuit. Also, the breakdown voltage of the single diode rectifier is limited which could affect the power handling capability of the circuit. Thus, an improved configuration, a Dickson-Greinach N=1 rectifier is proposed and shown in Figure 14.

The Dickson-Greinach N=1 (order 1) rectifier circuit is known as a half-wave voltage doubler [18]. It consists of a voltage source, two pairs of diodes, two capacitors and a load resistor.

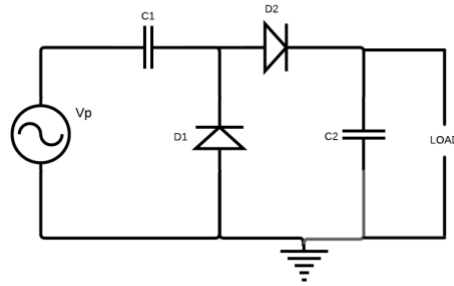


Figure 14: Half Wave Voltage Doubler (Dickson-Greinach N=1) [18].

During the negative half-cycle, diode D1 is biased and conducts charge to capacitor C1 until the value of the input voltage (V_i) is obtained. As there is no return path for C1 to discharge, C1 acts as a storage device with the supply voltage. At the same time, diode D2 conducts across D1 charging capacitor C2.

During the positive half cycle, diode D1 is reverse biased blocking the discharge of C1 while diode D2 is forward biased charging capacitor C2. But since there is a voltage across capacitor C1 that is already equal to the input peak voltage, capacitor C2 is charged to twice the value of the input signal peak voltage. Then the voltage across capacitor C2 can be calculated as (3):

$$V_{C2} = V_{out} = 2V_i \quad (3)$$

This doubled output voltage is not instantaneous but increases slowly with each input cycle. As capacitor C2 is only charged for half a cycle, the output voltage at the load has a ripple frequency equal to the supply frequency, hence the name half-wave voltage doubler.

The advantage of this circuit is that it allows higher voltages to be created from a low-voltage power supply without the need for an expensive high-voltage transformer. This is because the voltage doubler circuit allows the use of a transformer with a lower step-up ratio than would be required if an ordinary full-wave supply were used. However, while voltage multipliers can boost the voltage, they can only supply low currents to a high-resistance ($+100\text{k}\Omega$) load because the generated output voltage quickly drops-off as load current increases.

The disadvantage of this is that it can be difficult to smooth out this large ripple frequency in much the same way as for a half wave rectifier circuit. Also, capacitor C2 must have a DC voltage rating at least twice the value of the peak input voltage.

Figure 15 shows the result of the output voltages of each capacitance.

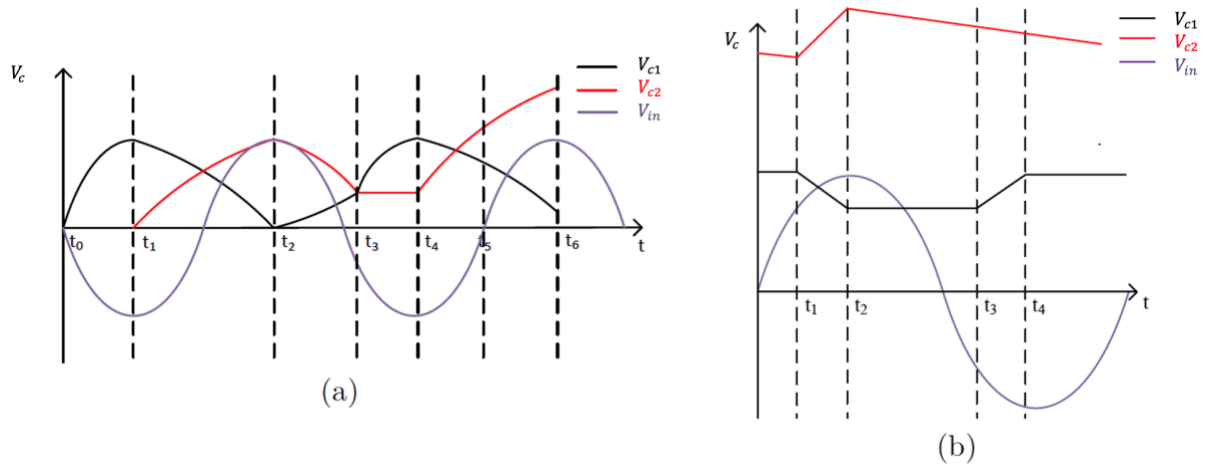


Figure 15: Waveform of voltage doubler [19].

In steady state and when the multiplier circuit is not loaded it is obtained that (2,3):

$$V_{C1} = V_m \quad (2)$$

$$V_{C2} = 2V_m \quad (3)$$

The voltage drop and voltage ripple will appear if the circuit is loaded with output load. At t_1 in Figure 19(b), the voltage source is in the positive switching cycle and rises to the certain value that fulfills the relationship of the equation (4):

$$V_{C1} + V_{in} = V_{C2} \quad (4)$$

As a result, D2 is conducting from t_1 to t_2 . C2 is charged and C1 is discharged until V_{in} increases to V_m at t_2 . At t_3 , the voltage source is in the negative switching cycle and decreases to the certain value that fulfills the following relationship (5):

$$V_{in} = -V_{C1} \quad (5)$$

As a result, D1 is conducting from t_3 to t_4 . C1 is charged by the voltage source. C1 and C2 are charged and discharged continuously in steady state.

2.5.4 Dickson N

The 2-stage Dickson rectifier is a variation of the traditional Dickson charge pump invented by John F. Dickson[20]. In the original design, shown in Figure 16, the charge pump acts as a DC-DC converter that uses two complementary synchronised input lines to move the load through each stage of the circuit. By grounding the DC input signal and grounding one of the clock lines, the circuit can become an RF rectifier.

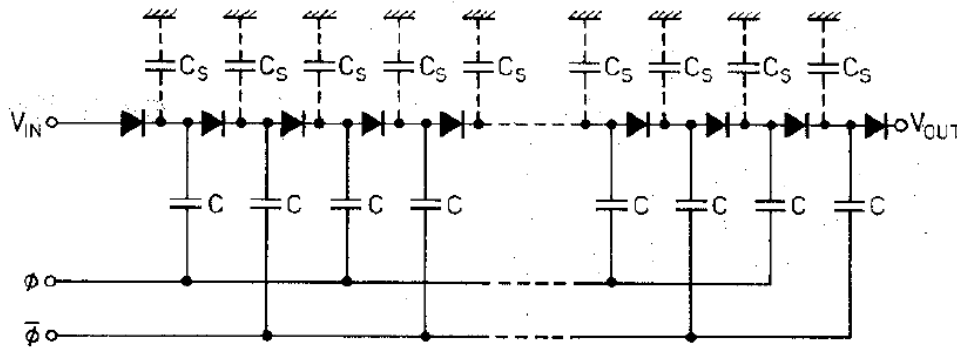


Figure 16: Original Dickson Charge Pump [20].

This modified version of the Dickson charge pump is shown in Figure 17, called the 2-stage Dickson. Two-stage multipliers are ideal for low power conditions. The number of stages used depends on the application and varies according to the method of implementation [21].

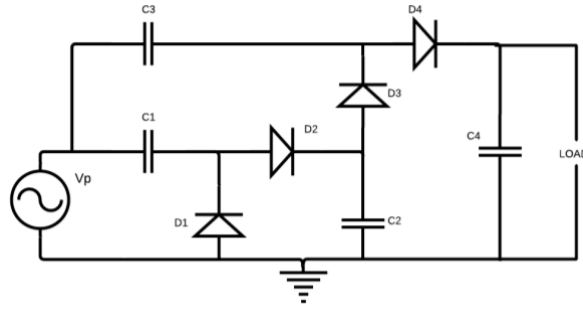


Figure 17: 2-Stage Dickson Charge Pump [21].

2.5.5 Greinach N=2

The Greinach N=2 rectifier circuit is known as a DC voltage quadruple circuit (Figure 18). Multiplier circuits are classified as doublers (such as the Dickson-Greinach rectifier), triples, quadruples, etc., depending on the ratio of output voltage to input voltage [22]. Any number of voltage multipliers can be obtained with a cascade of "N" doublers, which would produce an output voltage given by the following expression (5):

$$V_{out} = 2NV_p \quad (5)$$

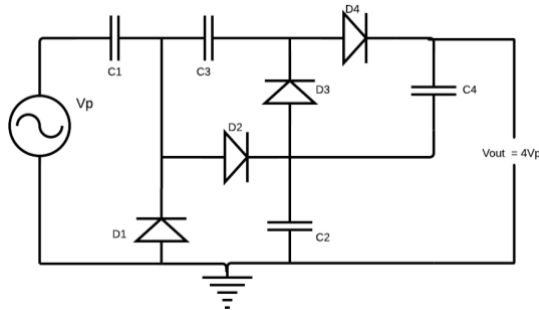


Figure 18: DC Voltage Quadrupler Circuit (Greinach N=2) [22].

The first voltage multiplier stage doubles the peak input voltage and the second stage doubles it again, giving a DC output equal to four times the peak voltage value ($4V_p$) of the sinusoidal input signal. Also, using large value capacitors will help to reduce the ripple voltage.

2.5.6 Full wave Dickson Variation

The full-wave Greinach rectifier circuit is equivalent to a two-stage voltage doubler circuit (The Dickson-Greinach $N=1$) formed in a bridge type, as can be seen in Figure 19.

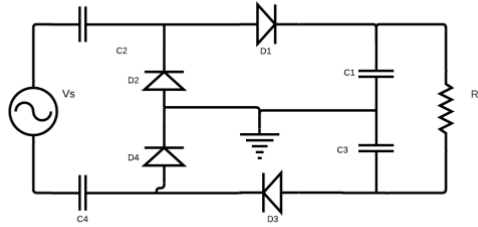


Figure 19: Configuration of the novel full-wave Greinacher rectifying circuit [23].

With this structure the overall RF power consumption is reduced, power sensitivity is improved, and good power handling capability is achieved using the full-wave rectification mechanism. The choice of diode is critical as the diode itself can be a major source of losses and directly affect the performance of the circuit [23].

3. Simulated and experimental results

This section will explain the set up used (physical and virtual) to measure the power available in the environment and analyse the different rectifier circuits previously explained in the theory. The results obtained for each rectifier circuit will also be analysed using the Keysight ADS program.

3.1 Set up

3.1.1 Spectrum analyser

A spectrum analyser is a device for measuring the frequency spectral density. In other words, it is a device that allows the size of an electromagnetic wave to be displayed with respect to frequency.

In this case, the Rohde Schwarz R&S®FSL model was used (Figure 20). This equipment works in a frequency range of 9 kHz and 6 GHz, collecting a maximum of 15,000 samples (enough precision to extract reliable data)[24]. It also has different options such as "trace mode" and "detector", which are configured and used in Section 3.3.



Figure 20: Spectrum analyser Rohde Schwarz R&S®FSL [24].

Figure 21 shows the block diagram of a spectrum analyser. It works as follows: the input signal passes through an attenuator, which is responsible for adjusting the value with respect to the desired reference level. Once this is achieved, the Low Power Filter rejects unwanted frequencies that could enter the mixer so that the desired signal is not distorted.

The Local Oscillation (LO) is used to convert the input signal to an Intermediate Frequency (IF). The LO is tuned by a Sweep generator to convert the entire input frequency range to a constant intermediate frequency.

The IF signal, the product of the desired signal with the LO signal, is amplified and fed to the IF filter with a Resolution Bandwidth (RBW) before it is fed to the diode detector. The detected signal is filtered by noise using a video filter before it is displayed. Depending on the frequency range set for the horizontal axis, the appropriate sweep time is calculated and used.

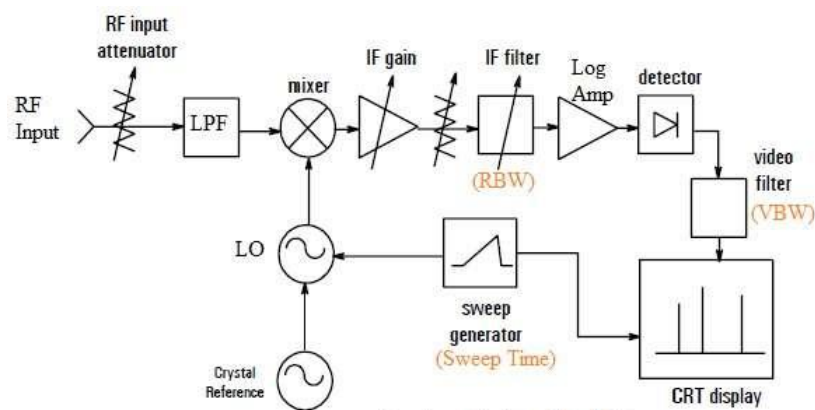


Figure 21: Block diagram of the spectrum analyser[25].

This equipment allows the user to choose the units in which to represent the measurements. On the abscissa axis the frequency (Hz) is represented and on the coordinate axis the level in dB, dBm, dB μ , dBmV, dBc... of the spectral content of the signal is represented on a logarithmic scale (Figure 22).

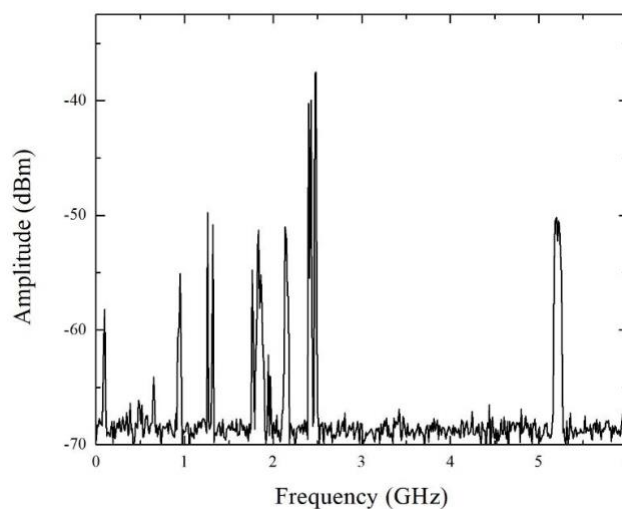


Figure 22: Spectrum analyser representation of the units on abscissa axis (frequency (Hz)) and coordinate axis (dBm)[26].

Decibels are a logarithmic expression of the ratio between two power levels (6). When we talk about decibels, we refer to a label because it is not a unit, if you want to talk about a quantity, you must have a reference (Watts, Volts...).

$$dB_{Magnitude} = 10 * \log\left(\frac{P_1}{P_2}\right) \quad (6)$$

It is understood as:

- dBm → Unit of electrical energy in decibels with reference in milliwatts(mW).
- dBμ → Unit of electrical energy in decibels referenced in microwatts(μW).
- dBmV → Unit of voltage in decibels referenced in millivolts(mV).
- dBc → Decibel in relation to the carrier power level.

The value is transformed directly by the spectrum analyser, but mathematically the dB to dBm transformation is obtained (1), where to find the value of P_1 (7) depends on the rms voltage which is given by the peak-to-peak voltage of the sinusoidal signal (8).

$$P_{1(mW)} = \frac{(V_{RMS})^2}{R} \quad (7)$$

$$V_{RMS(mV_{RMS})} = \frac{V_{PP}}{2\sqrt{2}} \quad (8)$$

The resistance value (R) is the impedance, which in the spectrum analyser is 50Ω.

The second power level (9) is defined by a reference value, usually 1 mW so that it can be expressed in dBm.

$$P_{2(mW)} = 1mW \quad (9)$$

Finally, with the conversions of (7)(9) the decibel value with quantitative unit (dBm) is obtained (6).

To work with voltages, the mathematical conversion from dB to dBmV requires the relationship between two voltages (11) starting from the main formula and assuming equal impedances.

$$dB_{Magnitude} = 10 * \log \left(\frac{\frac{V_1^2}{R}}{\frac{V_2^2}{R}} \right) = 10 * \log \left(\frac{V_1^2}{V_2^2} \right) \quad (10)$$

Finally,

$$dBmV = 20 * \log \left(\frac{V_1}{V_2} \right). \quad (11)$$

Understanding how the units that can be represented by the spectrum analyser work, in this work the frequency (Hz) will be used on the coordinate axis and on the abscissa axis it will be represented in power (dBm).

3.1.2 Antenna Model

For this project, an antenna model has been selected as a signal collector. The antenna used is a commercial model for tablet devices (Figure 23).



Figure 23: ANT-24-GHL90-SMA.

The antenna used is an ANT-24-GHL90-SMA (Annex I). It is a 50mm long, 90-degree omnidirectional whip antenna with $\frac{1}{4}$ wavelength. It is designed to work at a frequency of 2.4GHz. Table 2 shows the relevant antenna specifications.

Antenna	Characteristics					
	Dimensions	Central Frequency	Antenna Mounting	Gain	Input Impedance	Return Loss
ANT-24-GHL90-SMA	50.4X0.7 mm	2.4 GHz	SMA Connector	2dB	50 Ohm	-10dB @ 2.4GHz

Table 2: ANT-24-GHL90-SMA Antenna specification.

3.2 Virtual Set up

3.2.1 ADS

Keysight Advanced Design System (ADS) is used to make the practical study of the different rectifier circuits, with the data collected by the antenna and spectrum analyser.

The software provides an integrated design environment for designers of RF electronics products such as mobile phones, wireless networks, satellite communications, radar systems and others.

In addition, Keysight ADS supports every step of the circuit simulation design process in both the frequency domain and time domain, allowing an RF design to be fully characterised and optimised.

One of the tools that ADS has installed is Harmonic Balance (HB). It is a frequency domain analysis technique for simulating distortion in non-linear circuits and systems. For solving analogue RF problems, HB is the best method.

To perform a Harmonic Balance simulation, it is necessary to specify one or more fundamental frequencies and the order for each one. The simulator itself takes care of achieving near-optimal performance without the need to adjust any other parameters. The parameters to be highlighted are the following (Figure 24):

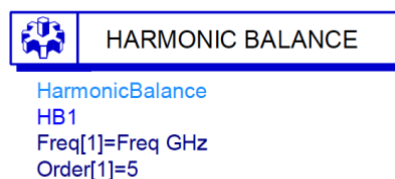


Figure 24: Configuration Harmonic Balance Parameters in Keysight ADS.

- Freq: Frequencies of fundamentals
- Orden [n]: Refers to the maximum order (harmonic number) of the fundamental frequencies under consideration. The number of harmonics must be large enough to represent non-linear signals. The lower the Order, the greater the HB truncation error. Any value below 5-7 may result in an error.

This configuration has been accompanied by a parameter sweep, which consists of a sweep of a variable (in this case the load resistance) and the implemented HB (Figure 25).

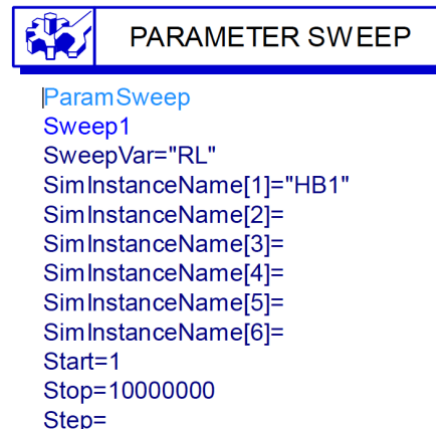


Figure 25: Configuration Parameter Sweep in Keysight ADS.

For this project, the HB of frequency 2.4 GHz and order 5 has been used together with the Parameter Sweep with a sweep in the load resistance for all the implemented circuits.

3.2.2 Estructure components ADS

Having explained what the ADS is and how it works, we proceed to explain the components needed for the rectifier circuits. These are:

- Diode

The diode used is model SMS7630_079 with a threshold voltage of 165mV and a breakdown voltage of 2V (Annex II). Figure 26 shows the characteristics implemented in the ADS.



Figure 26: ADS diode specifications.

Figure 27 considers the Schottky design model for the Harmonic Balance analysis, which takes into account DC and high frequencies.[27]

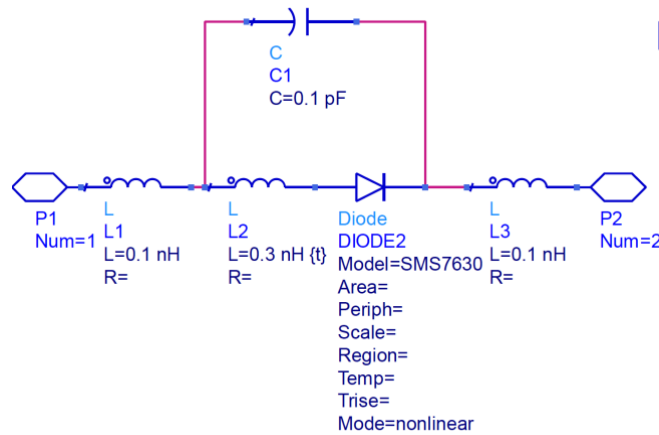


Figure 27: Schottky Design Model for the HB Analysis.

Note that P1 will be the RF input and P2 will be the RF output. Finally, the diode symbol is created (Figure 28).

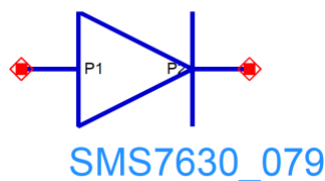


Figure 28: Symbol diode SMS7630_079.

- One tone power source

For the harmonic balance simulation, we need to place a one-tone power source (Figure 29). It will be placed at the RF input of the component.

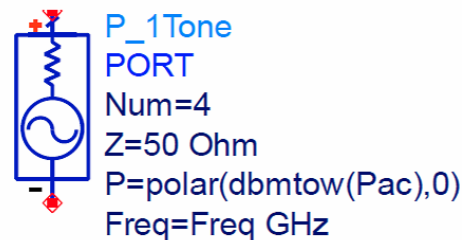


Figure 29: One Tone Power Source ADS.

Where Z is the source impedance, in this case is 50 Ohm. The variable P is the Power at centre frequency, which is used $\text{Polar}(\text{dbmtow}(\text{Pac}), 0)$. The dbmtow function takes care of passing the dBm to W. The value of Pac is -30dBm.

The frequency parameter is the fundamental frequency that will be tested. In this case we need 2.4GHz.

- Load Resistance

In rectifier circuits, a load resistor (Figure 30) is used in conjunction with the parameter sweep tool, which sweeps from 1Ω to $10\text{M}\Omega$.

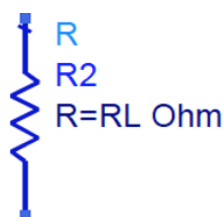


Figure 30: Load Resistance Symbol.

- Capacitance

For the rectifier circuits, a capacitance with a value of 4.7uF has been used (Figure 31).

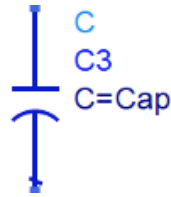


Figure 31: Capacity symbol.

Table 3 shows the summary of the variables used and the value of each one.

Variables	Valor
P_{AC}	-30 dB
Cap	4.7uF
Freq	2.4GHz
RL	3200
$L_{1,3}$	0.1nH
L_2	0.3nH

Table 3: Summary of the variables and each value in ADS.

3.3 Ambient available power for RF Harvesting

Before working with the different rectifier circuits, a study of the scenario in which we will be working has been carried out. The power of the environment available at the Autonomous University of Barcelona, specifically the power captured in the GAEMI laboratory of the UAB. Before starting with the measurements of the ambient power, some concepts about the frequency spectrum and the RF transmission frequency must be considered.

The first concept, the RF frequency spectrum band is classified into several categories: very high frequency (VHF), ultra-high frequency (UHF), super high frequency (SHF) and extremely high frequency (EHF), ranging from 3 kHz to 300 GHz [28].

RF transmission frequency, the second concept, can be divided into two main groups, which are uplink and downlink. For example, the transmission of power from a cellular phone to a base station is called uplink channel, while the transmission of power from a base station to a cellular phone is called downlink channel. The uplink and downlink frequency bands are different in duplex frequency division and can therefore be used separately for RF Energy Harvesting. Table 4 shows some of the most used RF frequency bands and their frequency ranges.

Frequency Band	Frequency Range (MHz)
VHF	30-300
FM	87.5-108
UHF	300-3000
TV	470-862
GSM900 UL	890-915
GSM900 DL	935-960
UMTS UL	1920-1980
UMTS DL	2110-2170
LTE UL	791-821, 880-915, 1710-1785, 1920-1980, 2500-2570
LTE DL	832-862, 925-960, 1805-1880, 2110-2170, 2620-2690
Wi-Fi	2400-2483.5
ISM	433, 915, 2450, 5800
5GNR Sub-6 GHz	3000-6000
5G mmWave	24000-30000, 37000-50000, 64000-71000, 95000-100000

Table 4: Common RF frequency bands and its respective frequency ranges [28].

In this case, the spectrum analyser has been configured to display the maximum peaks of the received signal (Maxpeak) and to maintain them from the beginning of the measurement (Maxhold) to visualise the spectral density of the maximum power captured with respect to the frequency (Table 5). It should be noted that a range of 6 GHz has been selected (maximum range allowed by the equipment) with a sampling of 2001 points (sufficient to obtain accurate data).

Center Freq	2.44652E9	Hz
Freq Offset	0	Hz
Span	2.04E8	Hz
x-Axis	LIN	--
Start	2.34452E9	Hz
Stop	2.54852E9	Hz
Ref Level	-20	dBm
Level Offset	0	dB
Ref Position	100	%
y-Axis	LOG	--
Level Range	100	dB
Rf Att	0	dB
RBW	3E6	Hz
VBW	1E7	Hz
SWT	0.01	s
Trace Mode	MAXHOLD	
Detector	MAXPEAK	
Sweep Count	0	
Trace 1:		
x-Unit	Hz	
y-Unit	dBm	
Preamplifier	OFF	
Transducer	OFF	
Values	2001	

Table 5: Spectrum analyser parameters for antenna characterisation.

A 24-hour sampling of the maximum energy of the environment has been performed. This means that, at some point in time, the spectrum analyser has detected these values at a certain frequency. In this way, it is possible to know what the maximum power in the environment at a is given time. This procedure is shown in Figure 32, which shows the maximum power peaks with respect to the frequency in the environment during 24h.

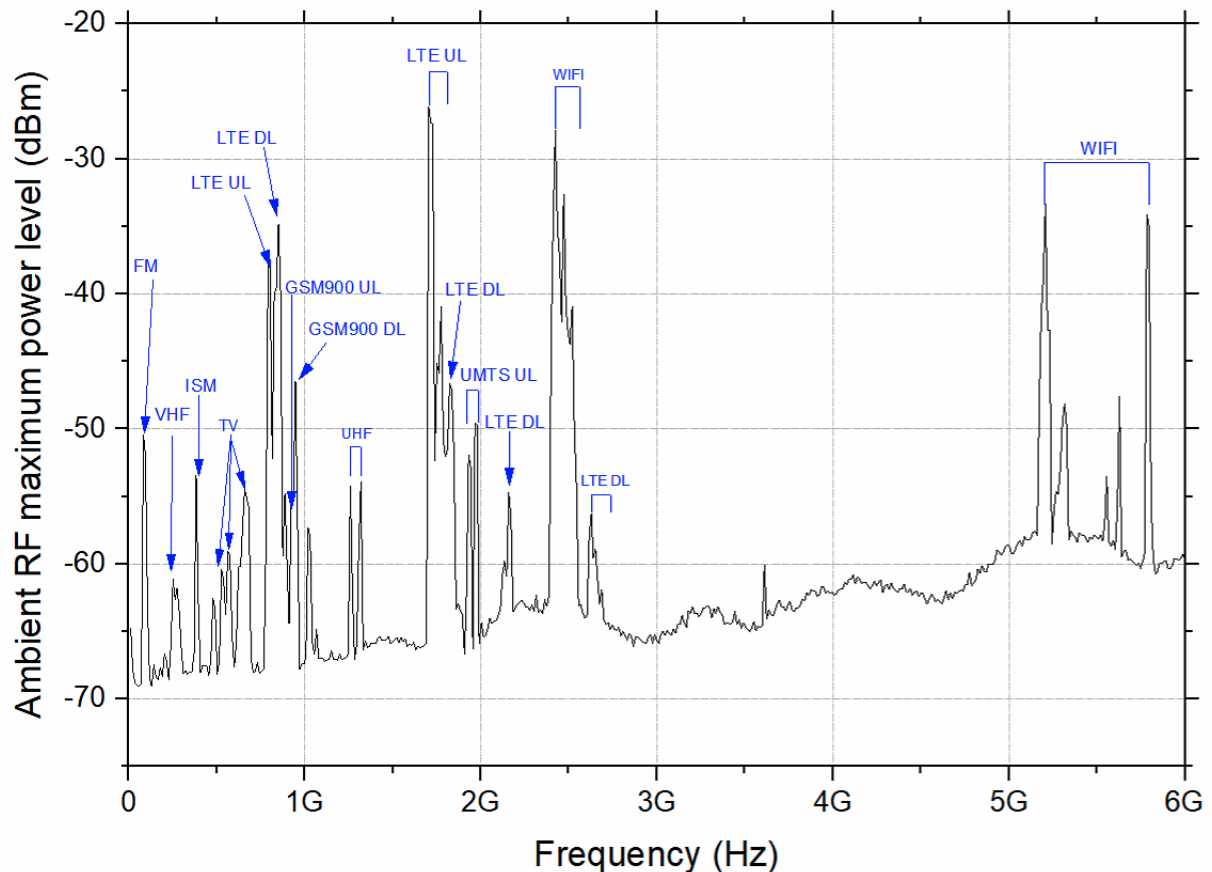


Figure 32: ANT-24G-HL90-SMA power capture over 24h with respect to frequency.

It has been decided to analyse the entire spectrum because, although the antenna used works mainly at the WIFI frequency, it is also interesting to analyse the frequencies of the environment, since any power detected by the antenna can be exploited.

Another aspect to highlight in Figure 34 is the frequency ranges where power peaks occur. This information can be useful for applications that have very specific frequency operating ranges.

Table 6 lists the above specifications. For example, if operating with a VHF RF power source and with a frequency in the range [30 MHz - 300 MHz], the emission power would be -30 dBm.

Sources of RF Energy	IF (MHz)	UF (MHz)	Frequency ranges (MHz)	Emission power levels (dBm)
VHF	30	300	165	-30
FM	87	108	97,5	-22.42
TV	470	862	666	-33.67
GSM900 UL	890	915	902.5	-48.54
GSM900 DL	935	960	947.5	-43.74
LTE UL	791	821	806	-37.32
	1710	1785	1747.5	-18.24
LTE DL	832	862	847	-38.02
	925	960	942.5	-45.81
	1805	1880	1842.5	-50.59
Wi-Fi	2400	2483,5	2441.75	-29.59

Table 6: Emission power level measurements (dBm) for RF energy sources.

3.4 Rectifier Circuits Simulated Results

In this section, Keysight ADS software has been used to design the rectifier circuits introduced in the theoretical part. Also, together with ADS, Origin has been used to obtain the efficiency, voltage and load impedance respect to de input power..

As mentioned in section 3.2.2 above, the values of the components used in the design of these circuits have been fixed (table 3). It should be noted that, the fundamental frequency is set to 2.4GHz because this is the main frequency that the antenna works to capture the WIFI signal.

A power probe, P_probe2, has been implemented in each circuit, which is responsible for measuring the introduced power minus the bounced power. In other words, it measures the real effective incoming power.

Three graphs have been made for each circuit analysing the efficiency, the output voltage and the load impedance.

Considering that -30dBm is considered ultra-low power, this value has been fixed in the graphs of the figures of the designed circuits. To do this, markers have been used to help in analysing the behaviour of the parameters mentioned.

The aim of this analysis is to find the optimum rectifier circuit working at -30dBm.

- Simple Rectifier.

Figure 33 shows the simple diode capacitor rectifier.

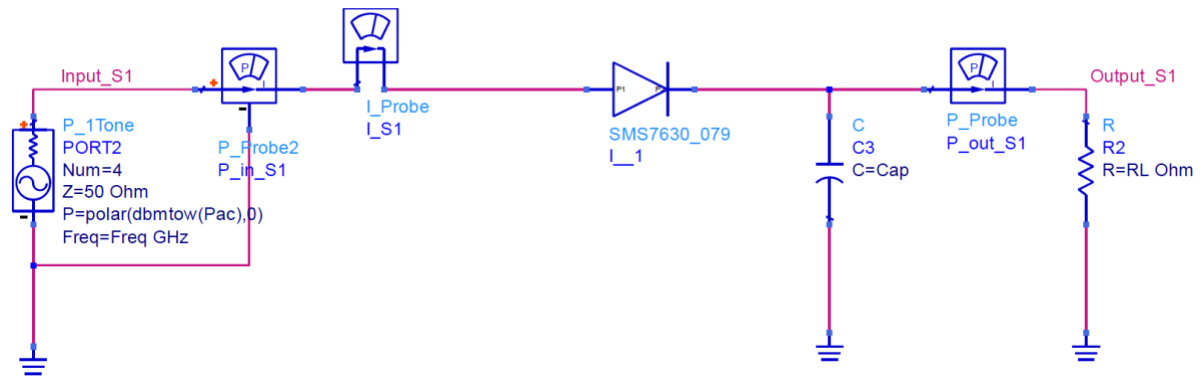


Figure 33: Simple Diode Capacitor Rectifier ADS.

Figures 34(a) and 34(b) show the efficiency of the circuit with respect to the input power. Looking at Figure 34(a), depending on the value of the load resistance, the efficiency of the circuit varies significantly.

An example could be indicated by marker m1, which represents the maximum value of the load resistance (6.310 k Ω) needed to obtain the highest efficiency (12.778%) of the circuit at an input power of -30dBm. In contrast, the m2 marker represents one of the worst values (631k Ω) for the same input power as an efficiency of 0.7% is obtained. Also, the maximum efficiency of the circuit can be observed in the marker m3, with 66.867%. Even so, the required input power is -4dBm (insufficient if working at ultra-low power).

Figure 36.b shows the topographical map of Figure 34(a) If a load resistance between 1k Ω and 10 k Ω is added, the maximum available efficiency is obtained. On the other hand, for any other value of load resistance, the efficiency would be between 0% and 6%.

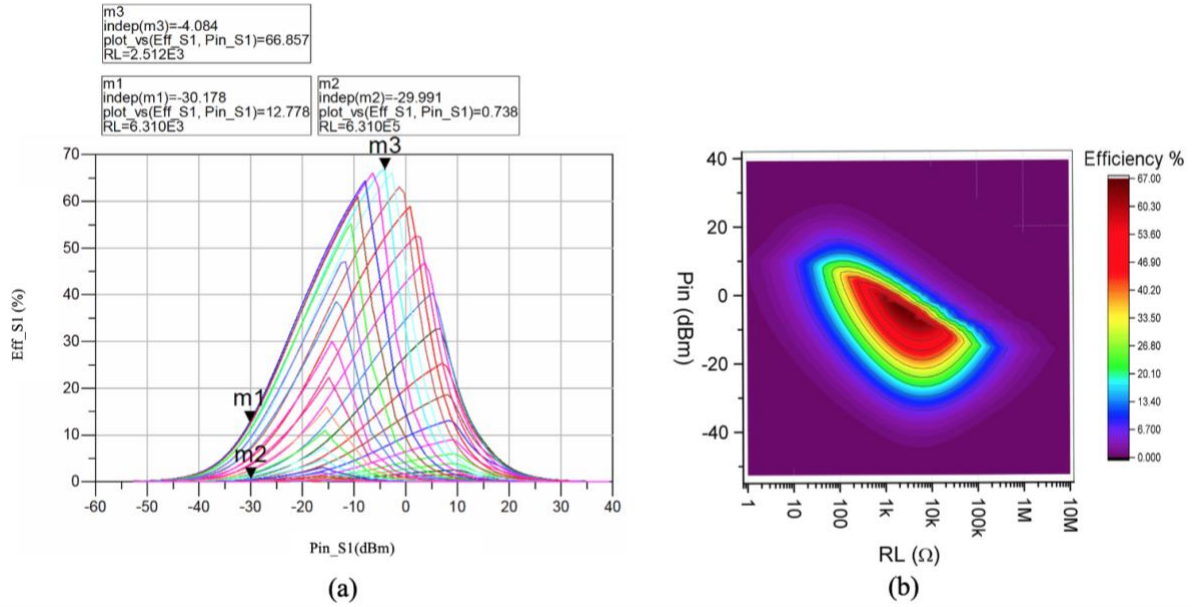


Figure 34: a) Representation (simple rectifier) of the efficiency with respect to the input power for each value of the load resistance. b) Topographical efficiency map for the simple rectifier.

Figure 35(a) show the output voltage versus input power.

It can be seen that, for -30dBm, the voltage is minimum for any value of the load resistor. The maximum voltage required is shown in marker m1 in Figure 35(a), which has a value of 0.065V.

Figure 35(b) represents the topographical map of graph (a). It can be distinguished that for a very large input power (between 10 and 40 dBm), the maximum applied voltage is obtained from a load resistance of 1 k Ω .

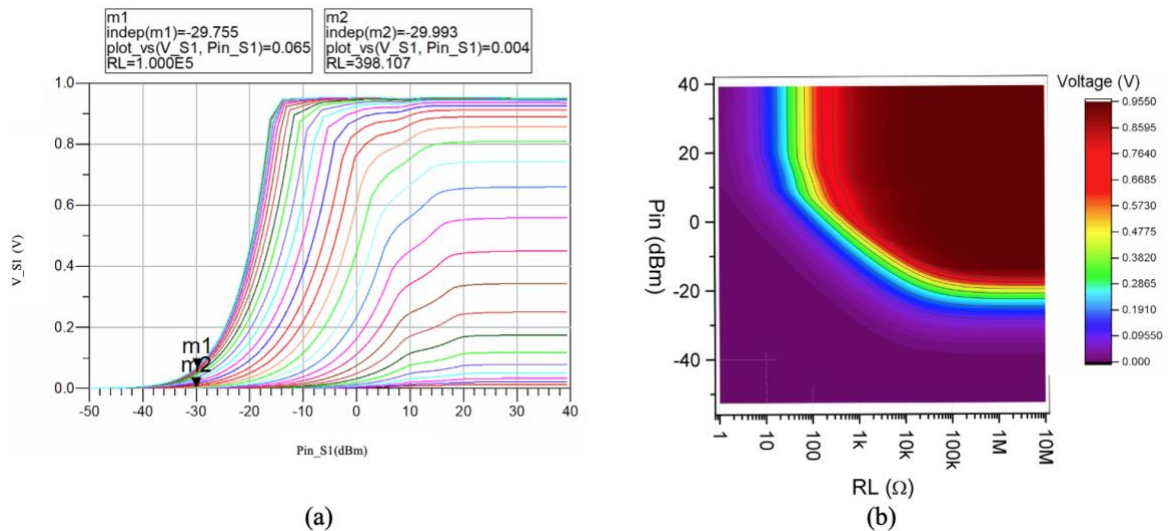


Figure 35: a) Representation (simple rectifier) of the output voltage with respect to the input power for each value of the load resistance. b) Topographical voltage map for the simple rectifier.

Figure 36 shows the input impedance, magnitude (top) and phase (bottom), with respect to the input power. Note that for a power of -30dBm, the value of the load resistance does not affect the impedance significantly, but it can be important from -20dBm up to 10 dBm. The markers m1-m2 and m3-m4 show the maximum and minimum of the magnitude and phase respectively.

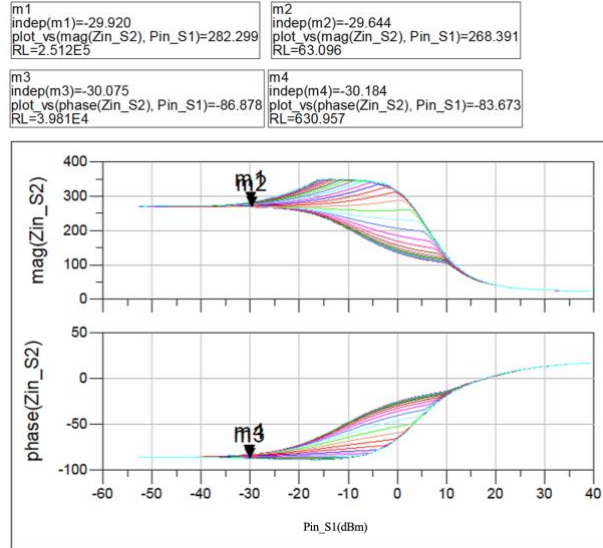


Figure 36: Representation of simple rectifier input impedance (magnitude (top) and phase (bottom)), with respect to the input power.

- Bridge.

Figure 37 shows the implemented bridge rectifier. The points marked B_input+ and B_input- are used to calculate the input voltage that is picked up by this diode bridge.

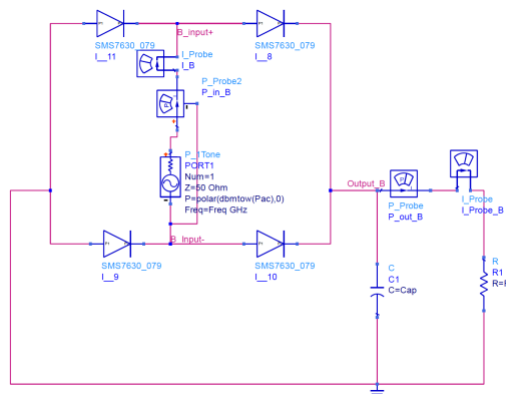


Figure 37: Bridge Rectifier ADS.

As explained in the previous case, Figures 38(a) and 38(b) show the efficiency of the circuit with respect to the input power.

At a glance, it is easy to see that the topographic map in Figure 38(b), has the same behaviour as the previous case (simple rectifier). The values of the load resistance to obtain maximum efficiency at -30dbm are between 1k Ω and 10k Ω . Marker 1 shows the maximum value of the load resistance (3.9k Ω) to obtain the highest efficiency of the circuit, which is 4.397%. In contrast, marker 2 shows another value within the optimum range for efficiency.

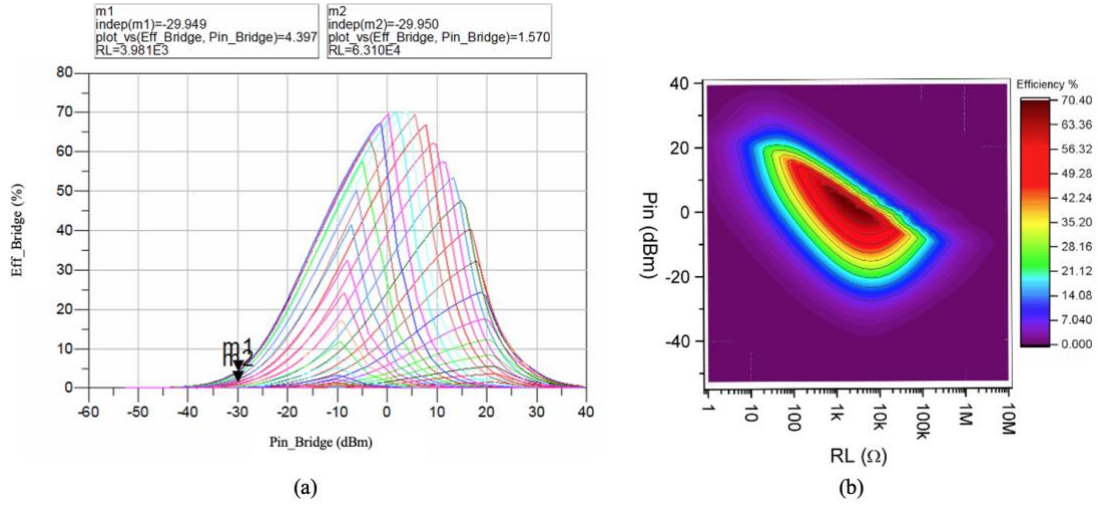


Figure 38: a) Representation (Bridge rectifier) of the efficiency with respect to the input power for each value of the load resistance. b) Topographical efficiency map for the Bridge rectifier.

Figures 39(a) and 39(b) show the output voltage versus input power. Markers 1 and 2 represent the maximum and minimum for the -30dBm case. The required output voltage is minimal, but as the input power increases, the voltage rises to 1.9V.

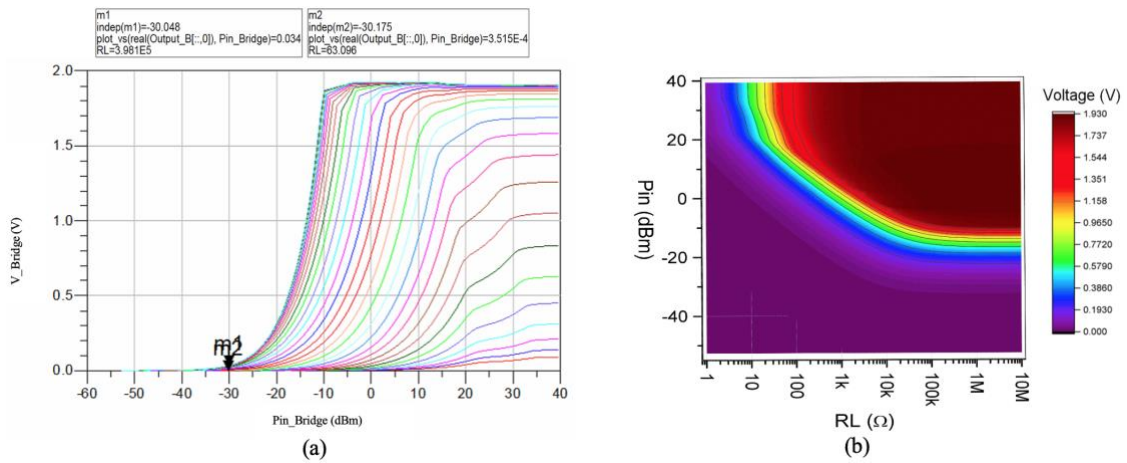


Figure 39: a) Representation (Bridge rectifier) of the output voltage with respect to the input power for each value of the load resistance. b) Topographical voltage map for the Bridge rectifier.

Figure 40 shows the input impedance, magnitude (top) and phase (bottom), with respect to the input power. It can be seen that for a power of -30dBm the value of the load resistance does not affect the impedance in a relevant way, but it can be important from -10dBm onwards. The markers m1-m2 and m3-m4 show the maximum and minimum of the magnitude and phase respectively.

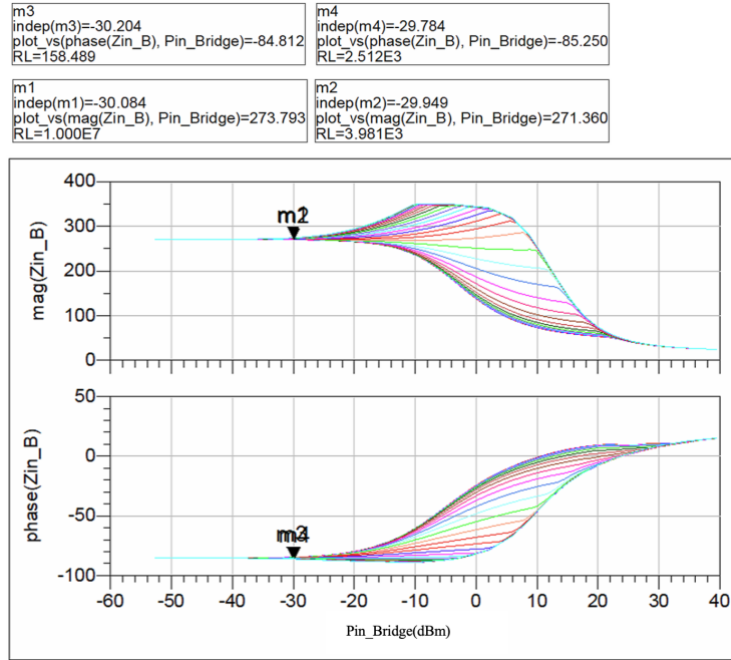


Figure 40: Representation of Bridge rectifier input impedance (magnitude (top) and phase (bottom)), with respect to the input power.

- Dickson- Greinach N=1.

Figure 41 shows the implemented Dickson-Greinach rectifier.

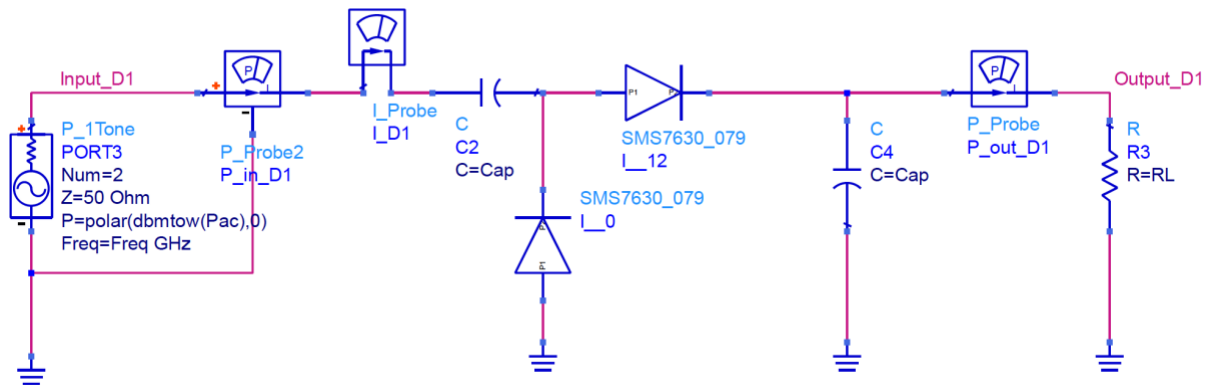


Figure 41: Dickson- Greinach N=1 Rectifier.

Observing the topographic map (Figure 42(b)), it has the same typology as the other two rectifier circuits analysed. The values of the load resistance to obtain maximum efficiency at -30dbm are around 1k Ω and 10k Ω . Marker 1 shows the maximum value of the load resistance (2.5k Ω) to obtain the highest efficiency of the circuit, which is 7.750%. Marker 2 shows one of the minimum values within the range.

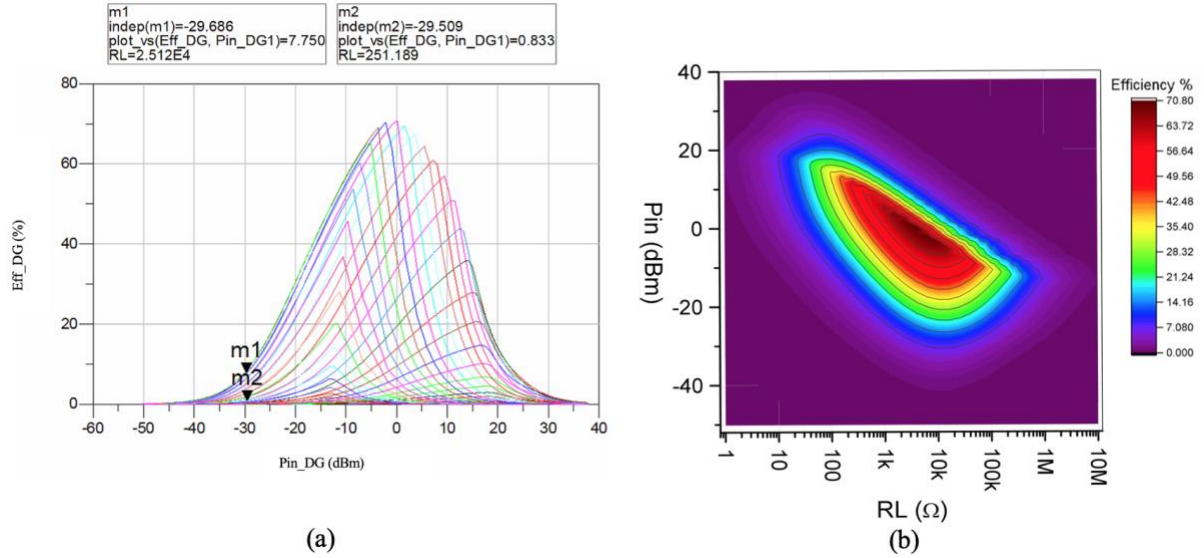


Figure 42: a) Representation (Dickson- Greinach rectifier) of the efficiency with respect to the input power for each value of the load resistance. b) Topographical efficiency map for the Dickson- Greinach.

Marker 1 and 2 in Figure 43(a) represent the maximum and minimum for the -30dBm case. The required output voltage is minimal (0.072V), but as the input power increases, the voltage shoots up to 1.9V.

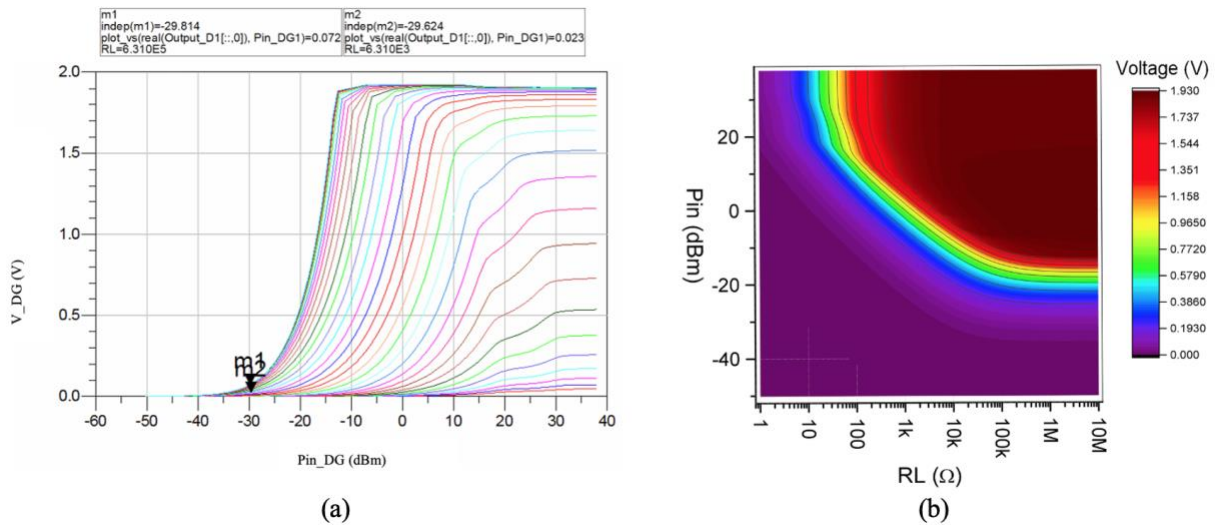


Figure 43: a) Representation (Dickson- Greinach rectifier) of the output voltage with respect to the input power for each value of the load resistance. b) Topographical voltage map for the Dickson- Greinach rectifier.

Figure 44 shows that for a power of -30dBm the value of the load resistance does not have a decisive impact on the impedance either. As pointed out above, the value of the resistance from -10dBm to 20dBm should be considered. The markers m1-m2 and m3-m4 show the maximum and minimum of the magnitude and phase respectively.

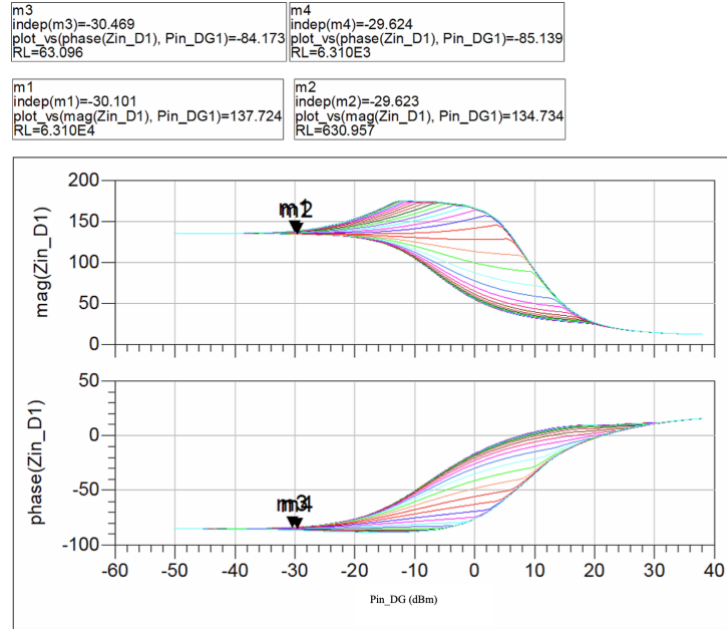


Figure 44: Representation of Dickson- Greinch rectifier input impedance (magnitude (top) and phase (bottom)), with respect to the input power.

- Dickson N.

Figure 45 shows the implemented Dickson N rectifier.

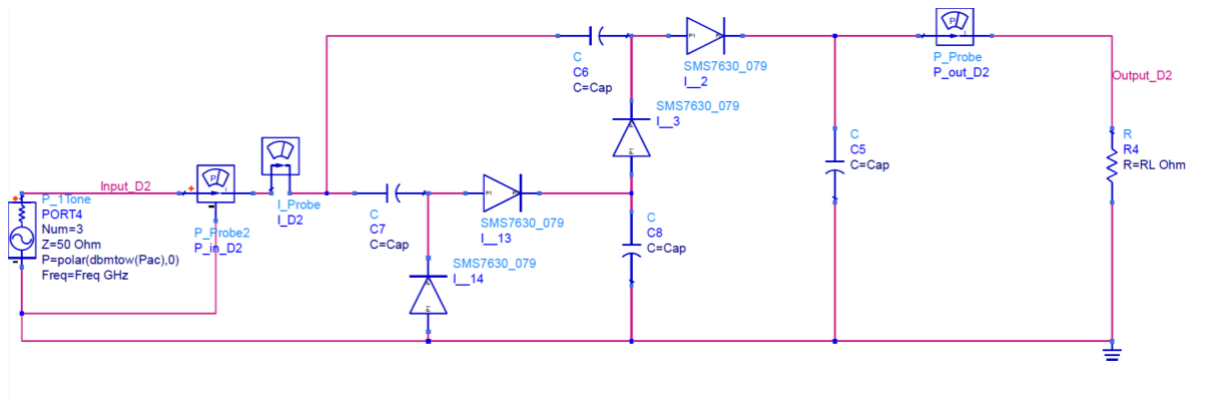


Figure 45: Dickson N rectifier ADS.

Figures 46(a) and 46(b) show the efficiency of the circuit with respect to the input power.

Observing the topographic map (figure 46(b)), it has the same typology as the previous rectifier circuits analysed. The values of the load resistance to obtain the maximum efficiency at -30dBm are around 10k Ω and 100k Ω . Marker 1 shows the maximum value of the load resistance (15.8k Ω) to obtain the highest efficiency of the circuit, which is 4.435%. Marker 2 shows the minimum value within the range.

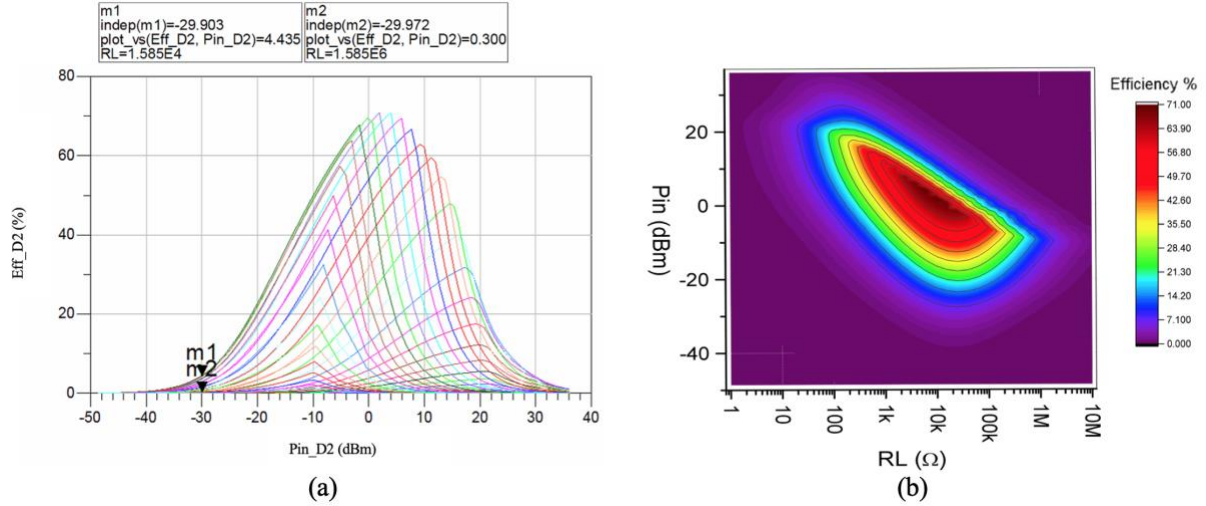


Figure 46: a) Representation (Dickson N rectifier) of the efficiency with respect to the input power for each value of the load resistance. b) Topographical efficiency map for the Dickson N.

Markers 1 and 2 represent the maximum and minimum for the -30dBm case (Figure 47). The required output voltage is minimal (0.082V), but as the input power increases, the voltage rises to 1.9V.

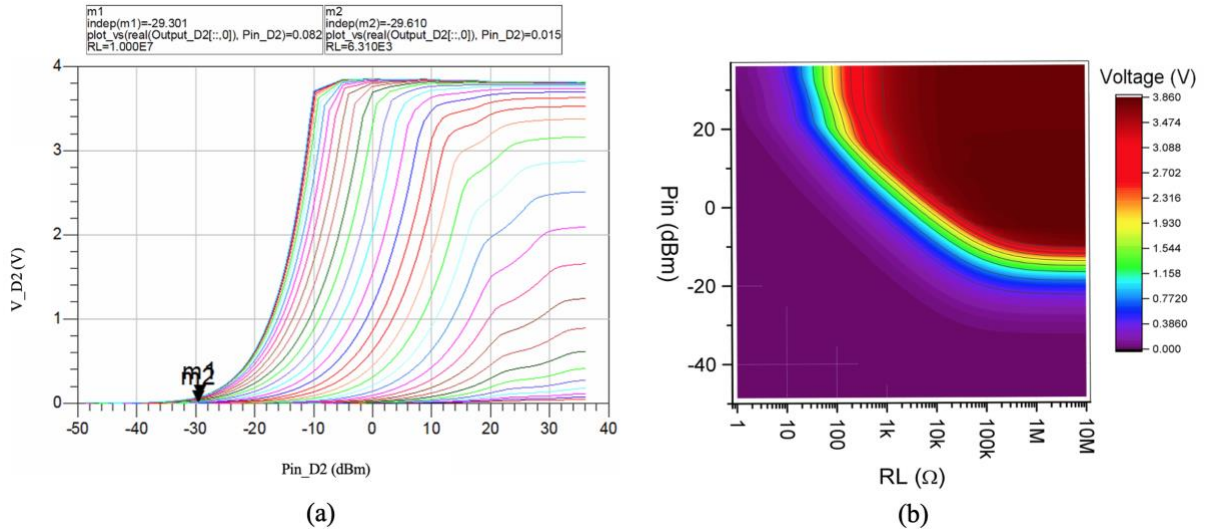


Figure 47: a) Representation (Dickson N rectifier) of the output voltage with respect to the input power for each value of the load resistance. b) Topographical voltage map for the Dickson N rectifier.

In Figure 48, it is observed that for a power of -30dBm the value of the load resistance does not noticeably affect the impedance. As in the previous models, the m1-m2 and m3-m4 markers show the maximum and minimum of the magnitude and phase respectively.

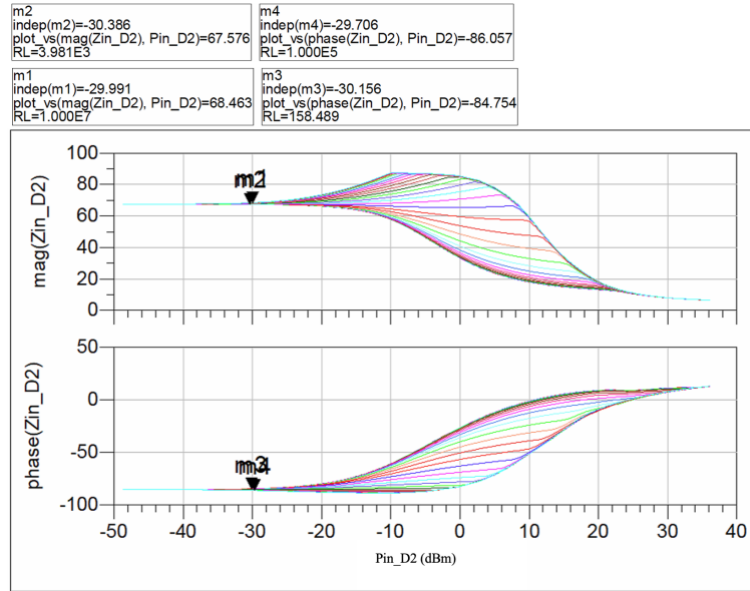


Figure 48: Representation of Dickson N rectifier input impedance (magnitude (top) and phase (bottom)), with respect to the input power.

- Greinach N=2.

Figure 49 shows the implemented Greinach N=2 rectifier.

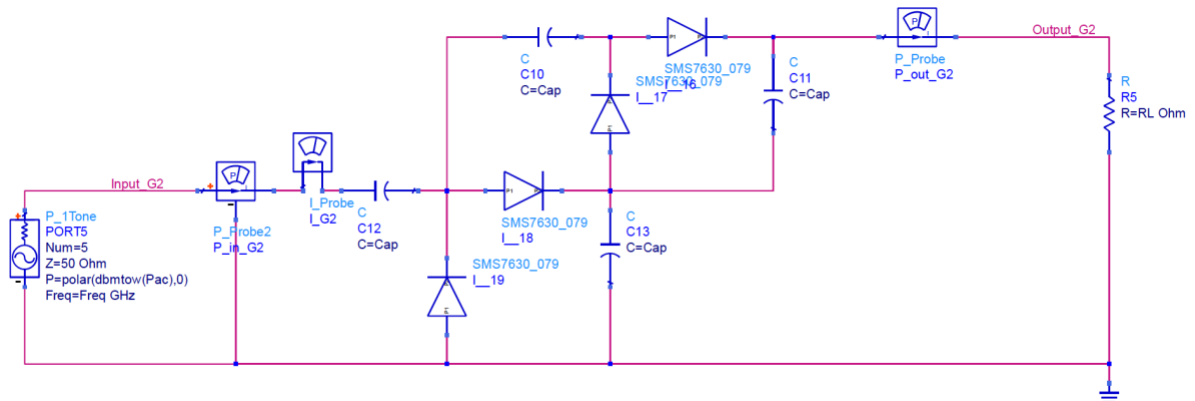


Figure 49: Greinach N=2 Rectifier.

As in the previous cases, Figures 50(a) and 50(b) show the efficiency of the circuit with respect to the input power. It can be seen that for this configuration, the response is the same as that of the Dickson N=2 rectifier circuit. The highest efficiency at -30dBm is marked by m1 in Figure 50(a).

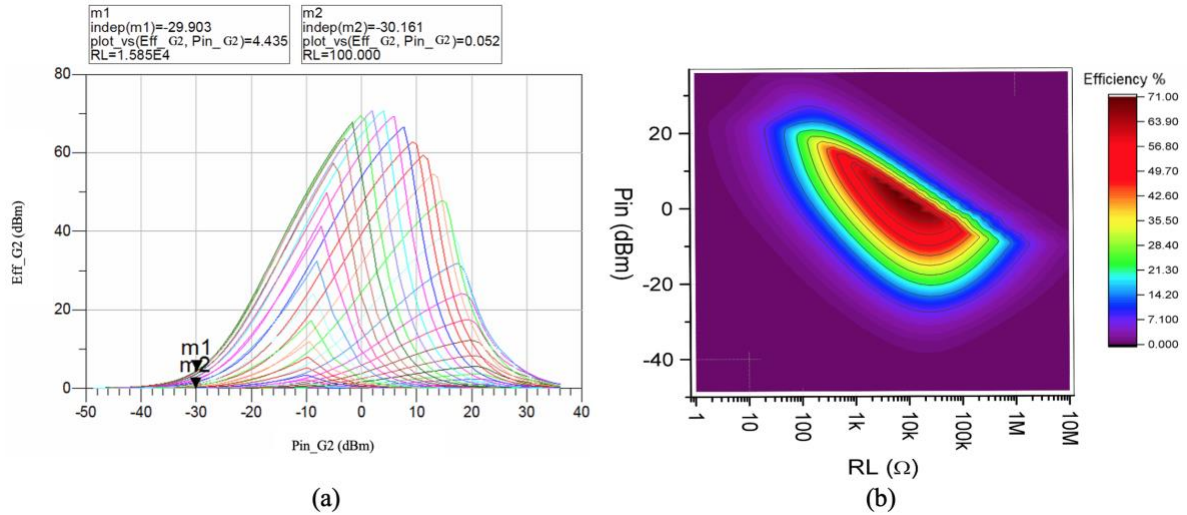


Figure 50: a) Representation (Greinach N=2rectifier) of the efficiency with respect to the input power for each value of the load resistance. b) Topographical efficiency map for the Greinach N=2.

Figure 51(a) and 51(b) shows the output voltage with respect to the input power. The marker 1 and 2 represent the maximum and minimum for the -30dBm case. The output voltage is the same as found in the previous circuit.

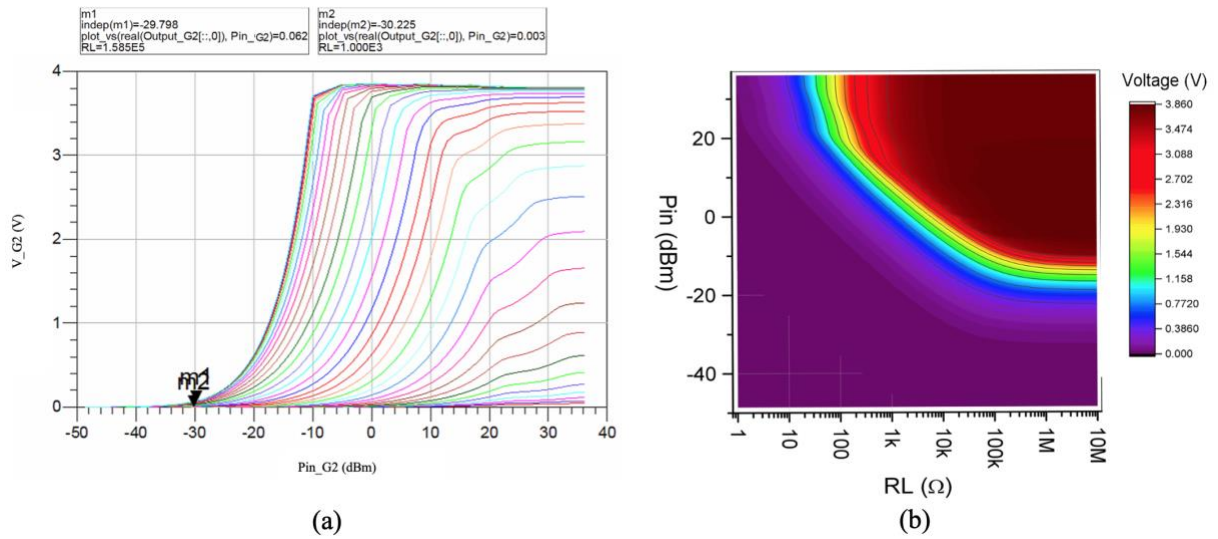


Figure 51: a) Representation (Greinach N=2 rectifier) of the output voltage with respect to the input power for each value of the load resistance. b) Topographical voltage map for the Greinach N=2rectifier.

Figure 52 shows the load impedance, magnitude (top) and phase (bottom), with respect to the input power. In this case, the graph obtained is the same as in the Dickson N=2 case.

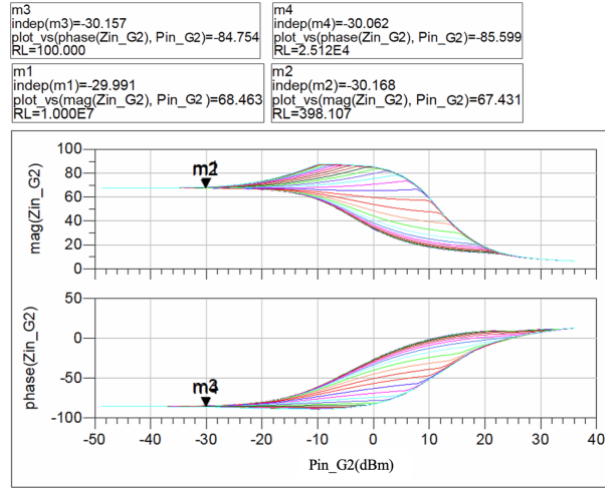


Figure 52: Representation of Greinach N=2 rectifier input impedance (magnitude (top) and phase (bottom)), with respect to the input power.

- Full wave Dickson Variation.

Figure 53 shows the implemented full wave Dickson Variation rectifier.

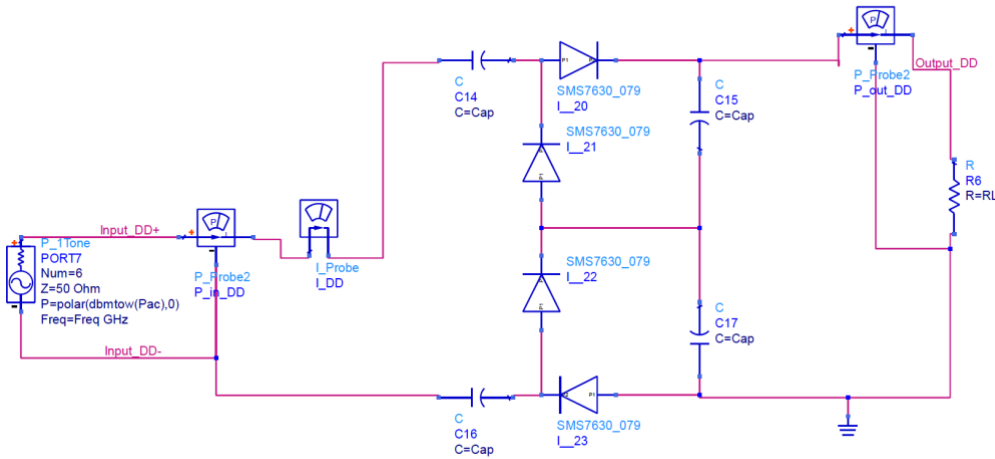


Figure 53: Full wave Dickson Variation rectifier.

Figure 54(a) shows a different behaviour than seen in the previous cases. Now the rectifier circuit is very inefficient when operating at ultra-low power. The marker m1 indicates the maximum efficiency that can be captured, which is only 1.65%.

In addition, the range of load resistances is very limited. It is worth noting that not only does it show very low efficiency in the -30dBm range, but also in the whole power band. Figure 54(b) shows the topographical map of the efficiency, which is also different from the cases seen so far.

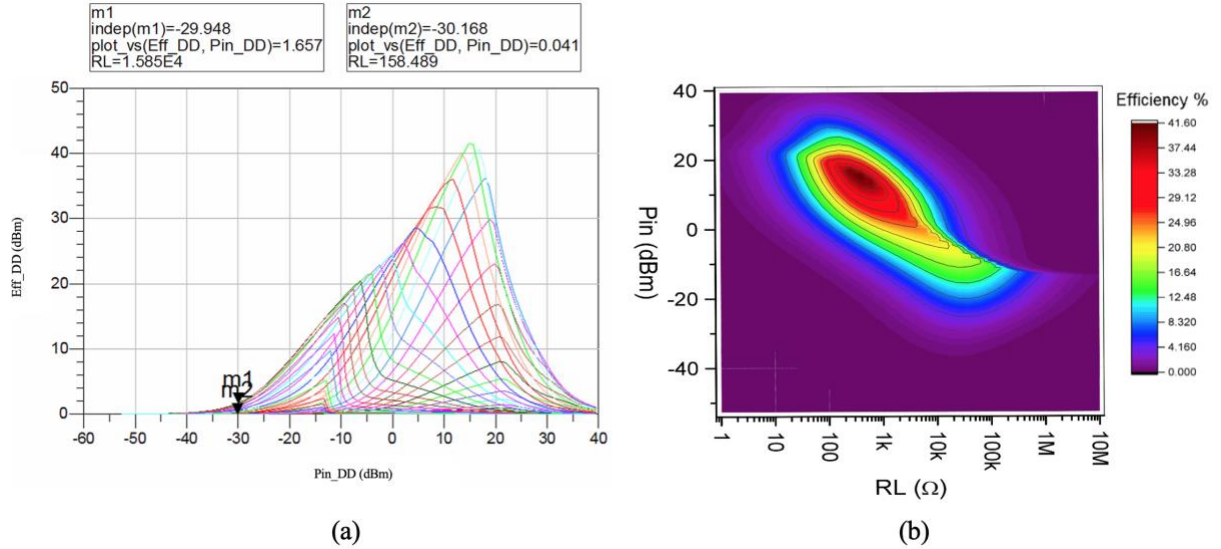


Figure 54: a) Representation (Full wave Dickson Variation rectifier) of the efficiency with respect to the input power for each value of the load resistance. b) Topographical efficiency map for the Full wave Dickson Variation.

Figure 55(a) and 55(b) shows the output voltage with respect to the input power. The marker 1 and 2 represent the maximum and minimum for the -30dBm case. The output voltage is the same as found in the previous circuit.

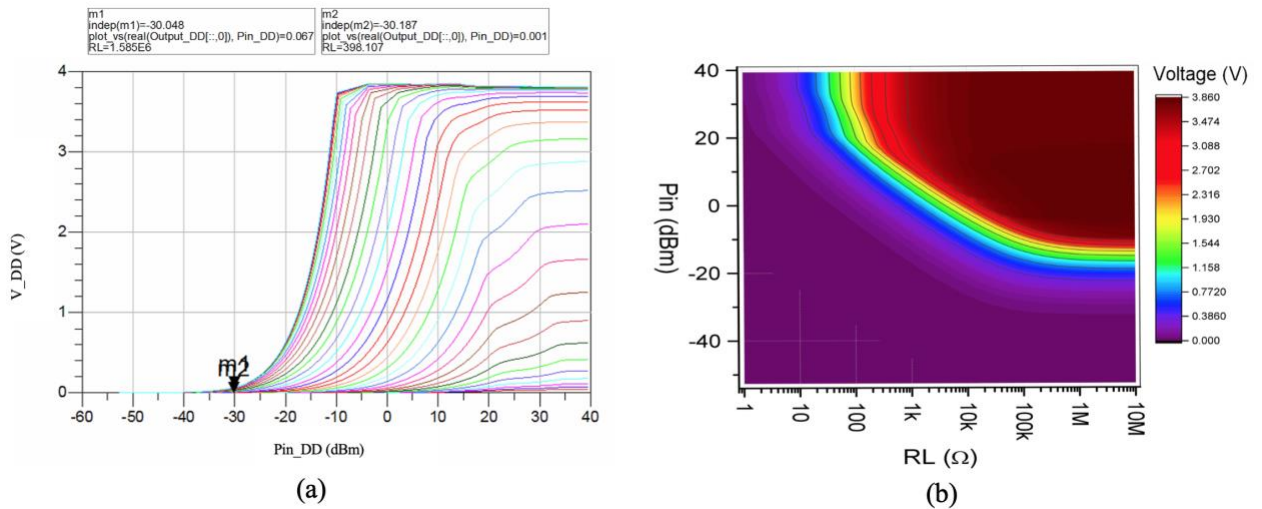


Figure 55: a) Representation (Full wave Dickson Variation rectifier) of the output voltage with respect to the input power for each value of the load resistance. b) Topographical voltage map for the Full wave Dickson Variation rectifier.

In Figure 56, it is observed that for a power of -30dBm the value of the load resistance does not noticeably affect the impedance. As in the previous models, the m1-m2 and m3-m4 markers show the maximum and minimum of the magnitude and phase respectively.

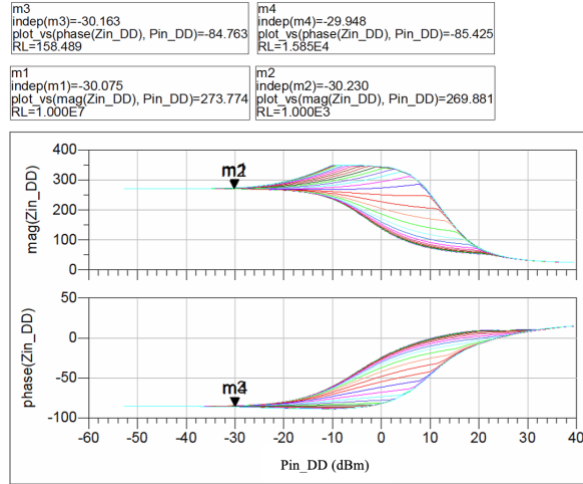


Figure 56: Representation of Greinach N=2rectifier input impedance (magnitude (top) and phase (bottom)), with respect to the input power.

4. Analysis and Discussion

In this section we will analyse the different results obtained from the rectifier circuits. To do so, a comparison will be made between them. Table 7 shows the topographical maps of the efficiency and voltage of each rectifier circuit. It has been chosen to show these two characteristics since it is here where the differences between circuits working at ultra-low power are most noticeable.

Regarding the efficiency topographical maps and centring the power at -30dBm, the simple rectifier was the circuit that simulated the best, with a maximum efficiency of 12.7%, applying a load resistance of 6.3k Ω . The second rectifier that showed a high efficiency was the Dickson-Greinach rectifier with 7.6% applying a load resistance of 15k Ω . The least efficient was the full wave Dickson variation with a maximum efficiency of 1.7%.

If the objective is to find the circuit capable of reaching the highest efficiency in any power band, Dickson and Greinach N=2 are the ones that achieve it as they have the same characteristics, with a maximum of 71% but with an input power of 0dBm (power of no interest in this work).

Analysing the output voltage topographic map, all the rectifier circuits show a very low voltage at the load resistor. This is because the value of the load resistor needed for -30dBm is very low.

If maximum efficiency is to be obtained at any power value, the single rectifier requires 0.9V at the output compared to the Full Wave Dickson variation which requires 3.9V.

Referring to the impedance plots in the previous section, it has been identified that the value of the input impedance does not significantly change no matter how large or small the value of the load resistor is.

Circuit Name	Topographic efficiency map	Topographic voltage map
Simple Rectifier		
Bridge		
Dickson-Greinach N=1		
Dickson N		
Greinach N=2		
Full wave Dickson Variation		

Table 7: Topographical representation of the efficiency and voltage of all implemented rectifier circuits.

Focusing on efficiency, which is the most critical element when working at ultra-low power, the element that makes the difference is the load resistance, as changing an order of magnitude can greatly influence the efficiency generated by the rectifier.

For this reason, the results of the efficiency of the rectifier circuits have been compared with other results obtained in other similar studies (Table 8). The first block of the table refers to the articles mentioned in the "Ref" column, and the second block refers to the data obtained in the ADS simulations. It should be noted that the sweep range of the RL is not large enough to have all the values and the closest value has been selected.

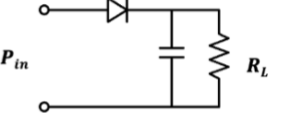
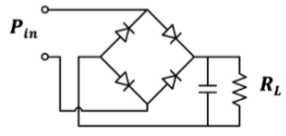
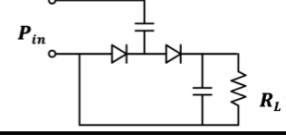
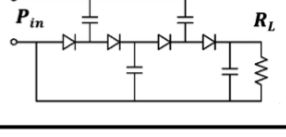
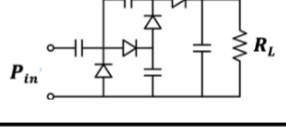
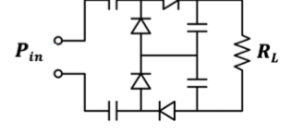
	Some example of common RF rectifier circuits operating @ 2.45 GHz				Comparison with the data obtained from the different rectifier circuits operating @ 2.45GHz			
	Ref	Pin	RL	Eff	Pin	RL	Eff	
Simple diode capacitor rectifier	[15]	-6.6 dBm	6 k Ω	48%	-6.1 dBm	6.3 k Ω	51.76 %	
	[29]	-15 dBm	1.7 k Ω	28%	-15dBm	1.5 k Ω	42%	
Bridge	[30]	-30 dBm	32 k Ω	8.8 %	-30 dBm	39 k Ω	1.9 %	
	[16]	-9.2 dBm	10 k Ω	68%	-9.17 dBm	10 k Ω	50.68 %	
	[31]	-7.6 dBm	500 k Ω	58%	-9.7 dBm	630 k Ω	5.17 %	
	[32]	-17 dBm	350 k Ω	50%	-17 dBm	398 k Ω	3.29 %	
Dickson-Greinacher N=1	[33]	-20 dBm	2 k Ω	5%	-20 dBm	2.5 k Ω	21.25%	
	[34]	-15 dBm	50 k Ω	20%	-15 dBm	63 k Ω	32%	
	[35]	-20 dBm	1 k Ω	17%	-19.88 dBm	1 k Ω	12.19 %	
Dickson N	[34]	-5 dBm	50 k Ω	70%	-5 dBm	63 k Ω	57%	
	[36]	5 dBm	5 k Ω	59%	5 dBm	6.3 k Ω	58%	
	[35]	-20 dBm	1 k Ω	5%	-20 dBm	1 k Ω	4.1%	
Greinacher N=2	[37]	13 dBm	20 k Ω	37.5 %	13 dBm	25 k Ω	2.50 %	
	[22]	-5 dBm	5 k Ω	10%	-5 dBm	6.3 k Ω	52%	
	[38]	-7.5 dBm	300 k Ω	9%	-5.22 dBm	398 k Ω	12%	
Full Wave Dickson Variation	[18]	9 dBm	6.7 k Ω	68%	8.7 dBm	6.3 k Ω	11%	
	[22]	-20 dBm	1.2 k Ω	6%	-20 dBm	1.5 k Ω	2.04%	
	[23]	-27.5 dBm	14.7 k Ω	5%	-27.5 dBm	15.8 k Ω	2.62%	
	[39]	-20 dBm	9 k Ω	12%	-20 dBm	10 k Ω	5.96%	

Table 8: Comparison with the data obtained from the different rectifier circuits operating @ 2.45GHz

It can be seen, in yellow, that the efficiency found differs quite a lot because the diode values or the elements used are different. Focusing on the ultra-low power data, when using the Bridge rectifier or the wave Dickson variation, the efficiency values do not differ much from the other articles.

Next, an analysis of the six rectifiers has been carried out for different load resistance values: 100Ω , $10k\Omega$ and $100k\Omega$. As seen in the topographical maps, the maximum efficiency for ultra-low power is achieved around the mentioned load values.

Figure 57 shows the efficiency of the rectifiers with respect to P_{nom} (Figure 57(a)) and P_{in} (Figure 57(b)) for a load resistance of $10k\Omega$.

The difference between the two graphical representations is that Figure 57(a) does not take impedance matching into account. Thus, much less power reaches the system as much of the captured energy is bounced back. As each circuit has a different input impedance, a consistent comparison between circuits cannot be made.

In contrast, in Figure 57(b), comparisons can be made between the different circuits because they all have the same value of matched impedance.

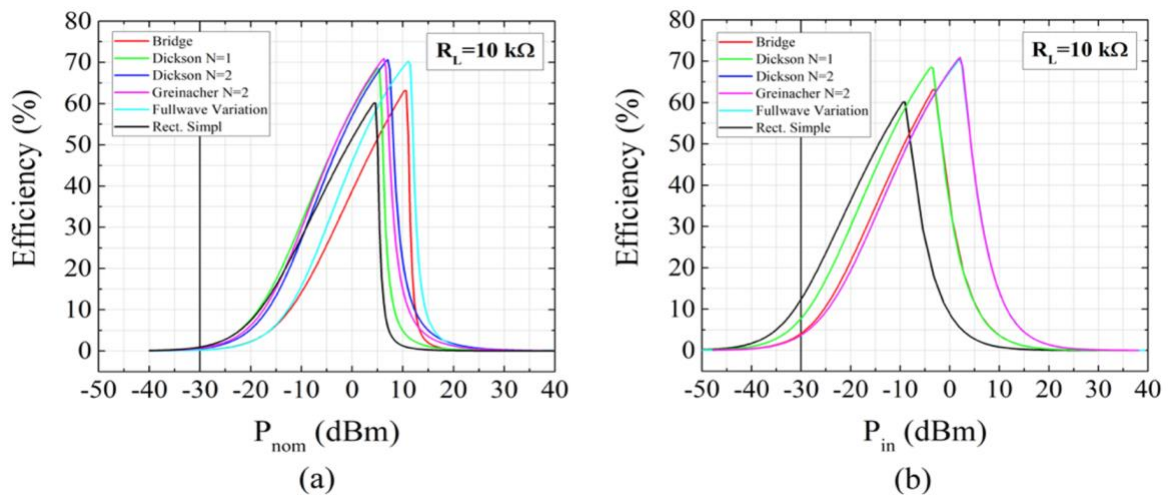


Figure 57: (a) Simulated rectifier efficiency for the six circuits of P_{nom} for a $R_L = 10\text{ k}\Omega$ (b) Simulated rectifier efficiency for the six circuits of P_{in} for a $R_L = 10\text{ k}\Omega$.

As can be seen, for a power of -30dBm the simple rectifier shows an efficiency of 12%, followed by the Dickson-Greinacher rectifier with an efficiency of 7% and the Bridge rectifier with 4%. The traces of the Dickson N=2, Greinacher N=2 and the full wave variation rectifier are overlapped, showing the same behaviour for the same load resistance value. Observing the behaviour of the simple rectifier, it can be said that it is the most optimal for low and ultra-low power. On the other hand, for powers higher than 0dBm, the more complex circuits show a better efficiency, reaching approximately 70%.

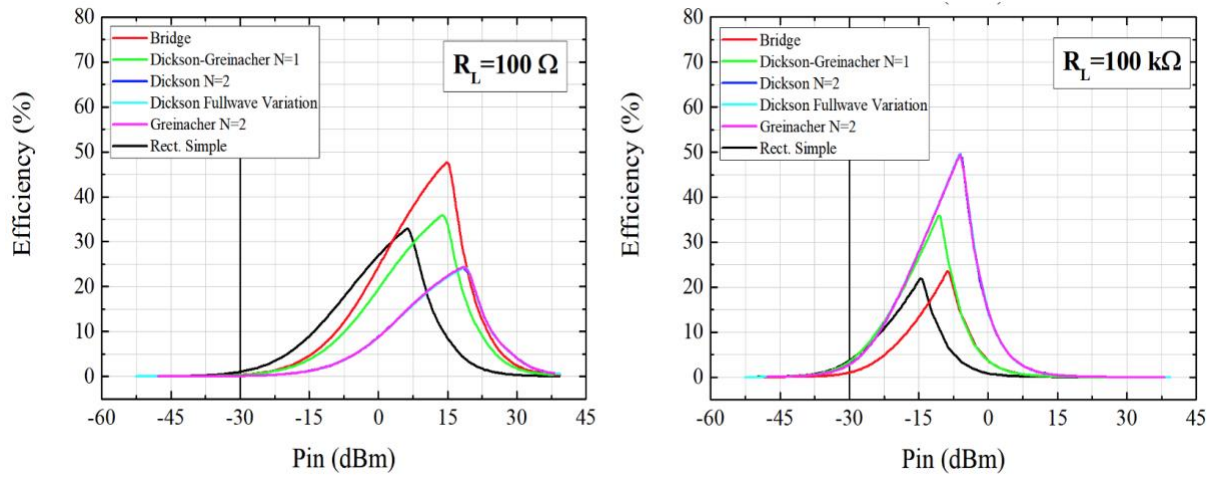


Figure 58: (a) Simulated rectifier efficiency for the six circuits of P_{in} for a $R_L = 100\Omega$. (b) Simulated rectifier efficiency for the six circuits of P_{in} for a $R_L = 100\text{ k}\Omega$.

Figures 58(a) and 58(b) show the power versus efficiency for a load resistance of 100Ω and $100\text{ k}\Omega$. Focusing on the ultra-low power, the performance of both graphs show a much lower efficiency than Figure 57(b) because the value of the optimum load is far away. Still, the simple rectifier adding a capacitance is the one that obtains the highest efficiency. For the case of $R_L = 100\Omega$ the efficiency for ultra-low power is less than 2%, although the highest efficiencies are the simple rectifier, the bridge and the Dickon-Greinacher. But for $P_{in} > 0\text{ dBm}$ power, the bridge rectifier achieves an efficiency of 47%.

For an R_L of $100\text{ k}\Omega$, all rectifiers show an efficiency for ultra-low power of less than 5%, yet the best performers are the single rectifier, Dickon-Greinacher and full wave variation. The circuits showing the best efficiency for $P_{in} > 0\text{ dBm}$ are the Greinacher N=2 and the full wave variation with 50%.

Both load resistors show a very low total efficiency compared to a $R_L=10\text{ K}$.

With the analysis focused on the optimal range of the load resistance, it has been demonstrated with simulations that to obtain maximum efficiency for $P_{in} = -30\text{dBm}$, a range around the load resistance of $10\text{K}\Omega$ is needed. To corroborate this study, experimental measurements have been taken of the three best rectifier circuits: the simple rectifier, the bridge rectifier and the Dickson-Greicacher rectifier.

Figure 59 shows the configuration of how the experimental results were obtained. A Decade box was used to generate the load resistance values and a vector analyser was used to generate a 50Ω monotone at a frequency of 2.45GHz with a power of -30dBm .

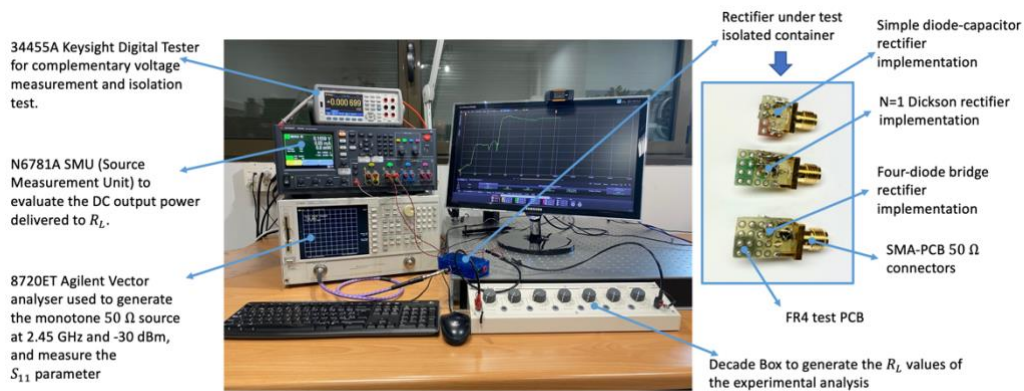


Figure 59: Experimental setup and details of the rectifier prototype implementation.

An SMU has also been used to measure the DC output voltage with a 4-wire measurement configuration with twisted wires. In this way, capacitive coupling is avoided and better measurement accuracy is obtained. Finally, the three implemented circuits have been used.

Figure 60 shows the efficiency with respect to load resistance of the three best rectifiers for an input power of -30dBm . The solid line shows the ADS simulated data and the dashed line formed by triangles shows the experimental measurement.

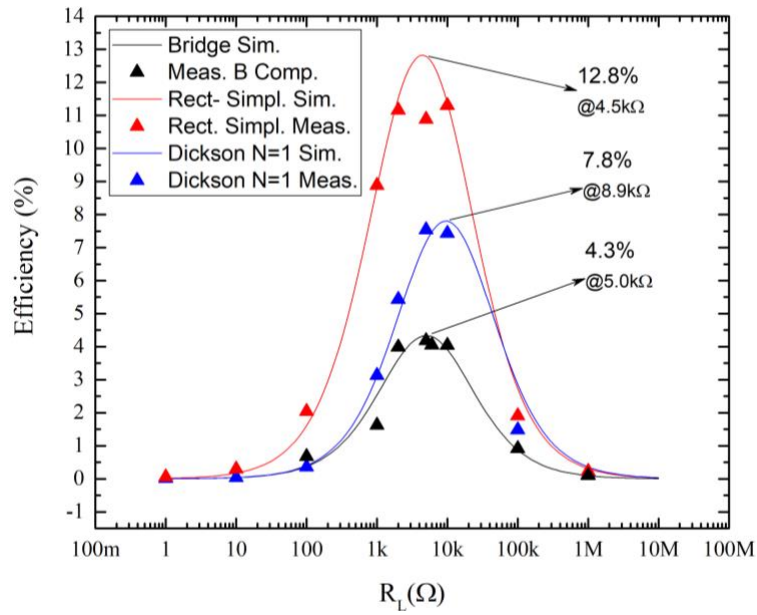


Figure 60: Representation of the efficiency of the simulated (solid line) and experimental (dashed triangle line) rectifiers with respect to the load resistance at a fixed power of -30dBm. The three circuits are the simple rectifier, the bridge rectifier and the Dickson-Greiner rectifier.

As can be seen, the actual value does not deviate from the simulated results. The simple rectifier shows the highest efficiency with 12.8% for a load resistance of 4.5k. This is followed by the Dickson-Greiner rectifier which has an efficiency of 7.8% for a load resistance of 8.9k. Lastly, the bridge rectifier with 4.3% for a load resistance of 5k.

5. Conclusion

It should be noted that the main objective of analysing and comparing different rectifier circuits used for ultra-low power RF Energy Harvesting in a realistic environment has been successfully completed.

The effects of the maximum power captured by the antenna in its different frequency bands have been analysed. This study can be of interest for devices that only work at certain frequencies.

Using ADS software, the efficiency, voltage, and input impedance (obtaining their topographic maps) have been simulated with respect to the input power of the six most common rectifier circuits for Energy Harvesting studies.

By solving the problem of impedance matching, it was possible to compare the rectifier circuits mentioned. This comparison has determined that the simple rectifier circuit is the one with the highest efficiency. It has also shown that the load resistance is a crucial element for obtaining good efficiency.

Finally, the results obtained in the simulations were compared with the experimental results. These confirm that the simple rectifier is the best for an input power of -30dBm.

The results of the present work can be continued in the analysis of complete Harvesting systems. On the other hand, some of the prototypes found in the literature could increase their efficiency by choosing a rectifier suitable for their environment.

6. References

- [1] J. Finnegan, K. Niotaki, and S. Brown, “Exploring the boundaries of ambient rf energy harvesting with lorawan,” *IEEE Internet of Things Journal*, vol. 8, no. 7, pp. 5736–5743, 2021, doi: 10.1109/JIOT.2020.3030349.
- [2] C. Delgado, J. M. Sanz, and J. Famaey, “On the feasibility of battery-less LoRaWAN communications using energy harvesting,” Dec. 2019. doi: 10.1109/GLOBECOM38437.2019.9013638.
- [3] N. Shariati, “Sensitive Ambient RF Energy Harvesting,” 2015.
- [4] S. Kim *et al.*, “Ambient RF energy-harvesting technologies for self-sustainable standalone wireless sensor platforms,” *Proceedings of the IEEE*, vol. 102, no. 11, pp. 1649–1666, Nov. 2014, doi: 10.1109/JPROC.2014.2357031.
- [5] L. G. Tran, H. K. Cha, and W. T. Park, “RF power harvesting: a review on designing methodologies and applications,” *Micro and Nano Systems Letters*, vol. 5, no. 1. Society of Micro and Nano Systems, Dec. 01, 2017. doi: 10.1186/s40486-017-0051-0.
- [6] G. Srinivasu, V. Kumar Sharma, A. Nella, V. Sharma, and N. Anveshkumar, “UMTS (2150-2200MHz), Wi-Fi(2.4-2.45GHz), Band for radio & television applications (900MHz-2GHz),” no. 4, 2019, [Online]. Available: <https://www.researchgate.net/publication/331975718>
- [7] S. Hemour and K. Wu, “Radio-frequency rectifier for electromagnetic energy harvesting: Development path and future outlook,” *Proceedings of the IEEE*, vol. 102, no. 11, pp. 1667–1691, Nov. 2014, doi: 10.1109/JPROC.2014.2358691.
- [8] “Campos Eletromagnéticos - Wangness, Roald K”.
- [9] G. M. de Arriba, E. Coskuner, and J. J. Garcia-Garcia, “Enhanced RF Harvesting System by the Utilization of Resonant Cavities,” in *2018 IEEE 28th International*

Symposium on Power and Timing Modeling, Optimization and Simulation, PATMOS 2018, 2018, pp. 29–31. doi: 10.1109/PATMOS.2018.8464175.

- [10] S. Hemour *et al.*, “Towards low-power high-efficiency RF and microwave energy harvesting,” *IEEE Transactions on Microwave Theory and Techniques*, vol. 62, no. 4, pp. 965–976, 2014, doi: 10.1109/TMTT.2014.2305134.
- [11] Y. Liu, K. L. Ren, H. F. Hofmann, and Q. Zhang, “Investigation of electrostrictive polymers for energy harvesting,” *IEEE Transactions on Ultrasonics, Ferroelectrics, and Frequency Control*, vol. 52, no. 12, pp. 2411–2417, Dec. 2005, doi: 10.1109/TUFFC.2005.1563285.
- [12] A. L. Yela and D. S. Vargas, “Multi-frequency microwave energy harvesting receivers: Theory and applications.”
- [13] E. Vandelle *et al.*, “Harvesting Ambient RF Energy Efficiently With Optimal Angular Coverage,” *IEEE TRANSACTIONS ON ANTENNAS AND PROPAGATION*, vol. 67, no. 3, pp. 1862–1873, 2019, doi: 10.1109/TAP.2018.2888957.
- [14] “Power Diodes used as Half-wave Rectifiers.” https://www.electronics-tutorials.ws/diode/diode_5.html (accessed Jan. 13, 2022).
- [15] Y. Y. Hu, S. Sun, H. Xu, and H. Sun, “Grid-Array Rectenna with Wide Angle Coverage for Effectively Harvesting RF Energy of Low Power Density,” *IEEE Transactions on Microwave Theory and Techniques*, vol. 67, no. 1, pp. 402–413, 2019, doi: 10.1109/TMTT.2018.2881127.
- [16] A. Karampatea and K. Siakavara, “Synthesis of rectenna for powering micro-watt sensors by harvesting ambient RF signals’ power,” *Electronics (Switzerland)*, vol. 8, no. 10, 2019, doi: 10.3390/electronics8101108.
- [17] “Full Wave Rectifier.” http://www.evaldate.in/lab1/pages/diode/DiodeFullwave/DiodeFullwave_T.html (accessed Jan. 13, 2022).

- [18] S. Chandravanshi and M. J. Akhtar, "An efficient dual-band rectenna using symmetrical rectifying circuit and slotted monopole antenna array," *International Journal of RF and Microwave Computer-Aided Engineering*, vol. 30, no. 4, pp. 1–15, 2020, doi: 10.1002/mmce.22117.
- [19] W. Qian, "Electrical Sustainable Energy Modeling and analysis of high frequency high voltage multiplier circuit for high voltage power supply Weijun Qian."
- [20] J. F. Dickson, "1976_On chip high voltage gen_Dickson," *IEEE JOURNAL OF SOLID-STATE CIRCUITS*, vol. SC-11, no. 3, pp. 374–378, 1976.
- [21] F. G. della Corte, M. Merenda, G. G. Bellizzi, T. Isernia, and R. Carotenuto, "Temperature effects on the efficiency of dickson charge pumps for radio frequency energy harvesting," *IEEE Access*, vol. 6, pp. 65729–65736, 2018, doi: 10.1109/ACCESS.2018.2876920.
- [22] R. Berges, L. Fadel, L. Oyhenart, V. Vigneras, and T. Taris, "Conformable dual-band wireless energy harvester dedicated to the urban environment," *Microwave and Optical Technology Letters*, vol. 62, no. 11, pp. 3391–3400, 2020, doi: 10.1002/mop.32461.
- [23] C. Song, Y. Huang, J. Zhou, J. Zhang, S. Yuan, and P. Carter, "A high-efficiency broadband rectenna for ambient wireless energy harvesting," *IEEE Transactions on Antennas and Propagation*, vol. 63, no. 8, pp. 3486–3495, 2015, doi: 10.1109/TAP.2015.2431719.
- [24] "NOISE FIGURE MEASUREMENT APPLICATION R&S®FSW-K30 R&S®FSWP-K30 R&S®FSMR3-K30 R&S®FSV3-K30 R&S®FPS-K30 R&S®FSV-K30 R&S®FPL1-K30."
- [25] "Block Diagram, Working and Applications of Spectrum Analyzer - Electronics Desk." <https://electronicsdesk.com/spectrum-analyzer.html> (accessed Jan. 13, 2022).

- [26] “ESCOLA TÈCNICA SUPERIOR D’ENGINYERIA (ETSE)-UAB Trabajo de Fin de Grado Realizado por: Guillem Martínez de Arriba.”
- [27] A. Y. Tang, V. Drakinskiy, K. Yhland, J. Stenarson, T. Bryllert, and J. Stake, “Analytical extraction of a schottky diode model from broadband S-parameters,” *IEEE Transactions on Microwave Theory and Techniques*, vol. 61, no. 5, pp. 1870–1878, 2013, doi: 10.1109/TMTT.2013.2251655.
- [28] L. Ramalingam *et al.*, “The Advancement of Radio Frequency Energy Harvesters (RFEHs) as a Revolutionary Approach for Solving Energy Crisis in Wireless Communication Devices: A Review,” *IEEE Access*, vol. 9. Institute of Electrical and Electronics Engineers Inc., pp. 106107–106139, 2021. doi: 10.1109/ACCESS.2021.3098895.
- [29] V. Palazzi *et al.*, “Design of a ultra-compact low-power rectenna in paper substrate for energy harvesting in the Wi-Fi band,” *2016 IEEE Wireless Power Transfer Conference, WPTC 2016*, pp. 23–26, 2016, doi: 10.1109/WPT.2016.7498823.
- [30] E. Coskuner and J. J. Garcia-Garcia, “Metamaterial impedance matching network for ambient rf-energy harvesting operating at 2.4 GHz and 5 GHz,” *Electronics (Switzerland)*, vol. 10, no. 10, pp. 1–14, 2021, doi: 10.3390/electronics10101196.
- [31] A. Karampatea and K. Siakavara, “Hybrid rectennas of printed dipole type on Double Negative Dielectric Media for powering sensors via RF ambient energy harvesting,” *AEU - International Journal of Electronics and Communications*, vol. 108, pp. 242–250, 2019, doi: 10.1016/j.aeue.2019.06.023.
- [32] Y. Chang, P. Zhang, and L. Wang, “Highly efficient differential rectenna for RF energy harvesting,” *Microwave and Optical Technology Letters*, vol. 61, no. 12, pp. 2662–2668, 2019, doi: 10.1002/mop.31945.
- [33] C. Song, Y. Huang, P. Carter, J. Zhou, S. D. Joseph, and G. Li, “Novel Compact and Broadband Frequency-Selectable Rectennas for a Wide Input-Power and Load

- Impedance Range,” *IEEE Transactions on Antennas and Propagation*, vol. 66, no. 7, pp. 3306–3316, Jul. 2018, doi: 10.1109/TAP.2018.2826568.
- [34] P. Li, Z. Long, and Z. Yang, “RF Energy Harvesting for Batteryless and Maintenance-Free Condition Monitoring of Railway Tracks,” *IEEE Internet of Things Journal*, vol. 8, no. 5, pp. 3512–3523, 2021, doi: 10.1109/JIOT.2020.3023475.
- [35] B. R. Marshall, M. M. Morys, and G. D. Durgin, “Parametric analysis and design guidelines of RF-to-DC Dickson charge pumps for RFID energy harvesting,” *2015 IEEE International Conference on RFID, RFID 2015*, pp. 32–39, 2015, doi: 10.1109/RFID.2015.7113070.
- [36] L. W. Cheng and G. Gnanagurunathan, “Two-Stage Dickson Charge Pump Rectifier with Harmonics Suppression for 2.45 GHz WPT,” *2020 IEEE International RF and Microwave Conference, RFM 2020 - Proceeding*, pp. 15–18, 2020, doi: 10.1109/RFM50841.2020.9344769.
- [37] S. Fan, Z. Yuan, W. Gou, S. Member, and Y. Zhao, “A 2.45-GHz Rectifier-Booster Regulator With Impedance Matching Converters for Wireless Energy Harvesting Shiquan,” *IEEE Transactions on Microwave Theory and Techniques*, vol. 67, no. 9, pp. 3833–3843, 2019.
- [38] J. P. Curty, N. Joehl, F. Krummenacher, C. Dehollain, and M. J. Declercq, “A model for μ -power rectifier analysis and design,” *IEEE Transactions on Circuits and Systems I: Regular Papers*, vol. 52, no. 12, pp. 2771–2779, 2005, doi: 10.1109/TCSI.2005.854294.
- [39] H. Zhang, Z. Zhong, Y. X. Guo, and W. Wu, “Differentially-fed charge pumping rectifier design with an enhanced efficiency for ambient RF energy harvesting,” *IEEE MTT-S International Microwave Symposium Digest*, vol. 0, pp. 613–616, 2017, doi: 10.1109/MWSYM.2017.8058642.

7. Annex

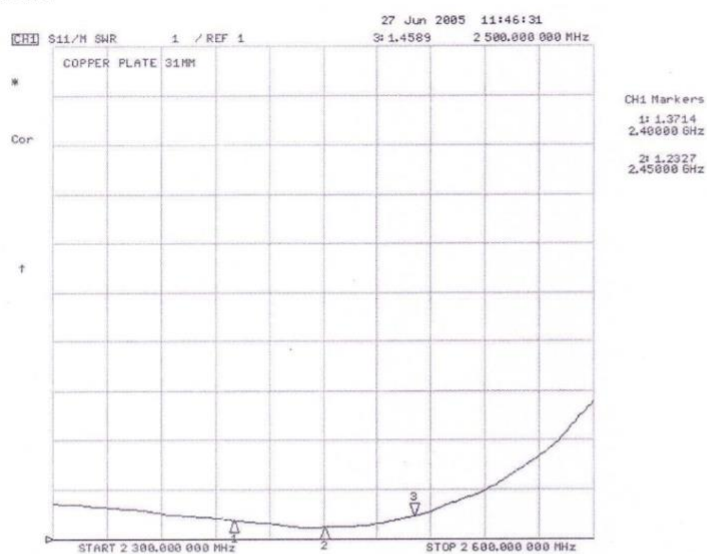
Annex I. Datasheet Antenna ANT-24G-HL90-SMA



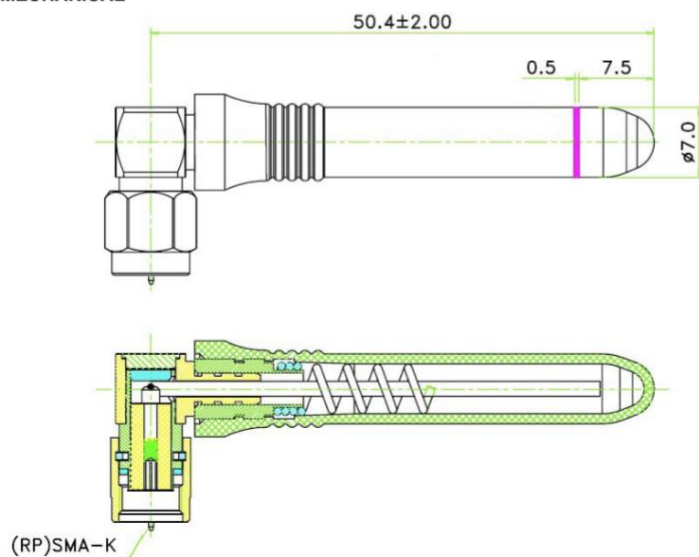
2.4GHz Antenna

ANT-24G-HL90-SMA

VSWR



MECHANICAL

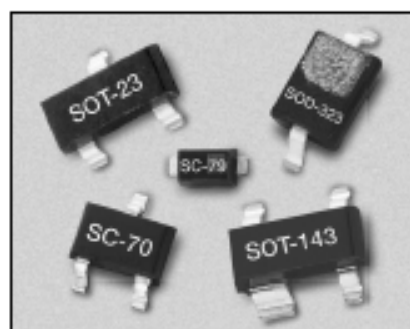


Surface Mount Mixer and Detector Schottky Diodes



Features

- Tight Parameter Distribution
- Available as Singles and Pairs
- 100% DC Tested
- Designed for High Volume Commercial Applications
- Available in Tape and Reel Packaging



Description

These low cost, surface mountable plastic packaged silicon mixer Schottky diodes are designed for RF and microwave mixers and detectors. They include low barrier diodes and zero bias detectors, combining Alpha's advanced semiconductor technology with low cost packaging techniques. All diodes are 100% DC tested and deliver tight parameter distribution, minimizing performance variability. They are available in SC-70, SC-79, SOD-323, SOT-23 and SOT-143 packages. Wiring configurations include singles, common cathode, series pairs and unconnected pairs. Applications include low noise receivers used in high sensitivity ID tags, wireless systems, radio designs and may be used at frequencies to 10 GHz. SPICE model parameters are included as a design tool.

Absolute Maximum Ratings

Characteristic	Value
Reverse Voltage (V_R)	Rated V_B
Forward Current - Steady State (I_F)	50 mA
Power Dissipation (P_D)	75 mW
Storage Temperature (T_{ST})	-65°C to +150°C
Operating Temperature (T_{OP})	-65°C to +150°C
Junction Temperature (T_J)	150°C
Soldering Temperature	260°C for 5 Seconds

Single	Single	Single	Common Cathode	Series Pair	Reverse Series Pair	Unconnected Pair	Reverse Unconnected Pair
SC-79	SOD-323	SOT-23		SOT-23	SOT-23	SOT-143	SOT-143
† SMS1546-011	† SMS1546-001			† SMS1546-005		† SMS1546-015	
Cathode Mark	Marking: SG1			Marking: SG2		Marking: SG7	
† SMS7621-079	† SMS7621-011	† SMS7621-001		† SMS7621-005	† SMS7621-006	† SMS7621-015	
Cathode Mark	Cathode Mark	Marking: SH1		Marking: SH2	Marking: SH8	Marking: SH7	
† SMS7630-079	† SMS7630-011	† SMS7630-001		† SMS7630-005	† SMS7630-006	$L_S = 1.5$ nH	† SMS7630-020
Anode Mark	Cathode Mark	Marking: SD1		Marking: SD2	Marking: SD8		Marking: SD0
$L_S = 0.7$ nH	$L_S = 1.5$ nH	$L_S = 1.5$ nH		$L_S = 1.5$ nH	$L_S = 1.5$ nH		$L_S = 1.5$ nH
			SC-70	SC-70	SC-70		
			† SMS7621-074	† SMS7621-075	† SMS7621-076		
			Marking: SH3	Marking: SH2	Marking: SH8		
				† SMS7630-075	† SMS7630-076		
				Marking: SD2	Marking: SD8		
			$L_S = 1.4$ nH	$L_S = 1.4$ nH	$L_S = 1.4$ nH		

† Available through distribution.

Electrical Specifications at 25°C (Per Junction)

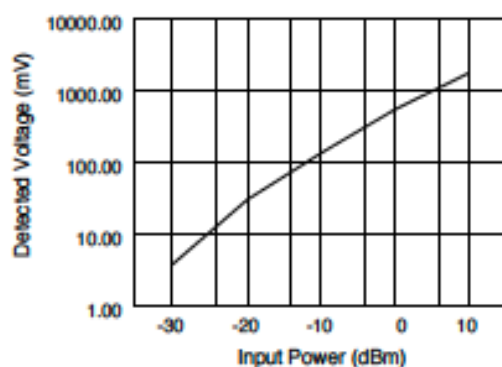
Low Barrier Mixer and Detectors

Part Number	Barrier	$V_B @ 10 \mu A$ (V)	$C_T @ 0 V$ (pF)	$V_F @ 1 mA$ (mV)	Pair Configuration (b) $V_F @ 1 mA$ (mV)	$R_T^* @ 10 mA$ (Ω)
		Min.	Typ.		Max.	Max.
SMS1546 Series	Low	2	0.50	200–270	10	8
SMS7621 Series	Low	2	0.25	260–320	10	18

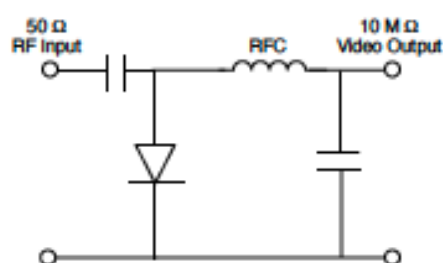
* R_T is the slope resistance.

Zero Bias Detectors

Part Number	$V_B @ 100 \mu A$ (V)	$C_T @ 0.15 V$ (pF)	$V_F @ 0.1 mA$ (mV)	$V_F @ 1 mA$ (mV)	Pair Configuration (b) $V_F @ 1 mA$ (mV)	R_V (Ω)
	Min.	Typ.			Max.	Typ.
SMS7630 Series	1.0	0.30	60–120	135–240	10	5000



Typical Detector
Characteristics @ 1.8 GHz



SPICE Model Parameters (Per Junction)

Parameter	Unit	SMS1546	SMS7621	SMS7630
IS	A	3E-7	4E-8	5E-06
RS	Ω	4	12	20
N		1.04	1.05	1.05
TT	S	1E-11	1E-11	1E-11
CJO	pF	0.38	0.10	0.14
M		0.36	0.35	0.40
EG	eV	0.69	0.69	0.69
XTI		2	2	2
FC		0.5	0.5	0.5
BV	V	3	3	2
Igv	A	1E-5	1E-5	1E-4
VJ	V	0.51	0.51	0.34